Marine and Petroleum Geology 130 (2021) 105112

Contents lists available at ScienceDirect

Marine and Petroleum Geology

journal homepage: www.elsevier.com/locate/marpetgeo

Research paper

An innovative method for the characterization of oil content in lacustrine shale-oil systems: A case study from the Middle Permian Lucaogou Formation in the Jimusaer Sag, Junggar Basin

Yazhou Liu [a,b], Jianhui Zeng [a,b,*], Guangqing Yang [a,b], Wanting Jia [a,b], Shengnan Liu [a,b], Xiangye Kong [a,b], Shengqian Li [a,b]

[a] State Key Laboratory of Petroleum Resources and Prospecting, China University of Petroleum (Beijing), Beijing, 102249, PR China
[b] College of Geosciences, China University of Petroleum (Beijing), Beijing, 102249, PR China

ARTICLE INFO

Keywords:
Potential favorable intervals
Shale oil systems
Shale oil composition
OCEI method
Jimusaer sag

ABSTRACT

Determination of oil content not only affects the exploration and development of potential favorable intervals in lacustrine shale-oil systems but also impacts research on the main factors controlling the differential accumulation of shale oil. Current approaches usually characterize a certain fraction of the hydrocarbons in shale oil. For example, the volatile hydrocarbon (S_1) fraction is considered to represent the hydrocarbons (C_7–C_{33}) that would be volatilized below 300 °C. In this article, an innovative method called the oil content evaluation index (OCEI) is proposed, in which the shale oil composition is considered and used to evaluate the vertical distribution of oil content utilizing conventional logging. In the OCEI method, the evaluation index (*LI**) represents the content of liquid hydrocarbons per unit mass of rock; this index successfully characterizes the discrete experimental data S_1 and chloroform extract yield. The evaluation index (*CI**) represents the oil-bearing area under the core description. The evaluation index (*GI**) characterizes the content of gaseous hydrocarbons in a constant volume. Based on the relationship between these evaluation indexes and the actual production, the relative weight of each evaluation index is determined through the grey relational analysis method. Finally, the OCEI value is the sum of the product of these normalized evaluation indicators and their corresponding weights. In a case study, the method is successfully implemented to predict the pay zones of the Lucaogou Formation in the Jimsar Sag, Junggar Basin, China. The threshold value of OCEI is set to 0.39 based on its relationship with production data. When the OCEI value of a certain interval is greater than 0.39, then this interval is a favorable pay zone. The evaluation results of two wells in the Jimusaer Sag further demonstrate that the model can effectively and reliably predict potential favorable intervals in shale oil systems.

1. Introduction

With increasing energy demand and the continuous consumption of conventional resources, unconventional resources are receiving greater attention as part of the global hydrocarbon endowment. Success in marine shale oil systems in North America has stimulated interest in efforts to produce oil from lacustrine shale oil systems in China (Gao et al., 2020; Hackley et al., 2016; Hu et al., 2020; Zhao et al., 2019, 2020). Shale oil resource systems are organic-rich mudstone units that have generated oil that is retained in situ or has migrated into juxtaposed organic-lean intervals (Jarvie, 2012). Based on their dominant organic and lithologic characteristics, shale oil systems are classified as (1) tight shale oil systems; (2) fractured shale oil systems; or (3) hybrid shale oil systems (Jarvie, 2012). The United States Energy Information Administration (EIA) (2015) estimated that technically recoverable resources of shale oil in China alone may stand at 4.37 billion tons, and in 2019, the China National Energy Administration preliminarily estimated that national recoverable shale oil resources range from 7.4 to 37.2 billion tons (Jin et al., 2019; Zou et al., 2020). Compared with the marine shale oil in North America, the lacustrine shale oil systems in China have unique characteristics of strong heterogeneity, low to moderate vitrinite reflectance, high viscosity, low production, high clay content, and other features (Du et al., 2019; Sun et al., 2019; Zhu et al., 2019). A few oilfields, such as Xinjiang, Changqing, Shengli, Daqing and

* Corresponding author. State Key Laboratory of Petroleum Resources and Prospecting, China University of Petroleum (Beijing), Beijing, 102249, PR China.
E-mail address: zengjh@cup.edu.cn (J. Zeng).

https://doi.org/10.1016/j.marpetgeo.2021.105112
Received 25 June 2020; Received in revised form 4 April 2021; Accepted 26 April 2021
Available online 12 May 2021

Tuha, have successfully begun shale-oil exploration and development research (Chen et al., 2015; Hu et al., 2018a,b; Huang et al., 2017; J. Li et al., 2015; Qiu et al., 2016a,b). The Xinjiang oilfield developed most rapidly. Although many shale-oil wells have been drilled in the Jimusaer Sag (Xinjiang oilfield), the initial production of shale oil is still highly variable. For example, the initial production of well J30 was 11.63 tons of oil per day, while well J23 had an initial production of 2.13 tons of oil per day (X. Wang et al., 2019; Xu et al., 2019). Although the source rocks and reservoirs of the formation have been characterized in numerous studies (e.g., Cao et al., 2016; Gao et al., 2016; Liu et al., 2019a,b; Zhao et al., 2017), relatively little research has focused on the evaluation of oil content. This is an essential component in evaluating potential shale-oil targets, resulting in considerable risks associated with assessing shale oil resources and designing optimized drilling, completion and development strategies.

Many researchers have established systematic methods for the evaluation of the oil content of shale oil systems (Glaser et al., 2013; Hakami et al., 2016; Jarvie, 2008; Ter Heege et al., 2015). These methods usually take into account the geological setting, organic matter composition, inorganic composition and pore characteristics. These indicators primarily include volatile hydrocarbon (S_1), total organic carbon content (TOC), and extractable bitumen contents, oil saturation index (OSI=S_1/TOC × 100), oil saturation (S_o) and $\sum nC_{20^-} / \sum nC_{21^+}$, and other parameters. The oil content of shale oil systems is influenced by the source rock and reservoir characteristics, effective conduits and thickness. Therefore, the oil content of "shale oil plays" should be evaluated to clarify whether the target can be effectively exploited and developed. Jarvie (2012) proposed that a shale interval could be identified as a viable petroleum reservoir when the oil saturation index (OSI) exceeded the retention threshold of 100 mg HC/g total organic carbon (TOC). This phenomenon is described as the "oil crossover effect". However, there are several issues with simply utilizing the threshold value. When the absolute values of S_1 and TOC are very low, the oil saturation index (OSI=S_1/TOC × 100) may be very high, greater than 100, and this could lead to a risk of uncertainty in the evaluation of shale oil resources. Based on the relationship between S_1 and TOC and on the oil saturation index value, W. Li et al. (2015) developed a new grading evaluation criteria that divided shale oil resources into four classifications: enriched resources (S_1 > 4 mg/g and OSI>100), moderately enriched resources (1 mg/g < S_1 < 4 mg/g and OSI>100), less efficient resources (1 mg/g < S_1 < 4 mg/g and OSI<100), and ineffective resources (S_1 < 1 mg/g and OSI<100). Hu et al. (2018a) proposed an improved method for the evaluation of lacustrine shale-oil resources that associated the organic type with grading evaluation criteria and used it to evaluate lacustrine shale-oil resources with strong heterogeneity. Li et al. (2020) proposed a new method called the "sweet spot index" (SSI) for predicting the vertical distribution of shale oil "sweet spots" based on shale oil mobility and shale reservoir fracability. This evaluation method, however, involves many indicators and is difficult to apply, so it has some limitations in the guidance of shale oil exploration and development. Besides, there are several issues with the utilization of the above data in the previous approaches. Some of these parameters are interrelated, such as volatile hydrocarbon (S_1), oil saturation and porosity, making the evaluation results of shale oil unclear. Secondly, due to the large thickness and vertical heterogeneity of lacustrine shale reservoirs, the limited core sample data are insufficient to explain the detailed information of the formation. Therefore, logging interpretation calibrated by core analysis is needed to predict the vertical distribution of oil content. Thirdly, without considering the relative importance of each variable, simply applying the sum or product of the normalized parameters that characterize the oil content as the evaluation standard of the pay zone, the prediction results may reflect only part of the oil content characterization (Li et al., 2020).

As an assemblage, crude oil and natural gas are widely distributed in source rocks and reservoirs. A shale-oil pay zone should have the feature of high liquid hydrocarbon content and high mobility (M. Wang et al., 2019). Therefore, an innovative method that associates oil content with mobility is proposed and utilized to predict potential targets in the Middle Permian Lucaogou Formation shale oil systems in the Jimusaer Sag, Junggar Basin. This method has several innovative features. First, it considers the two components of crude oil and natural gas, and it can determine the variation of vertical oil content in shale reservoirs with strong heterogeneity. Second, the value of OCEI is continuous combining logging data, laboratory analyses, core descriptions and oil production data. Third, the threshold value of the OCEI is finally determined based on the relationship between the evaluation results of oil content and shale oil production in the current research area. The effectiveness and reliability of the OCEI method are tested on two wells in the Jimusaer Sag.

2. Methods

Because the detection methods used to characterize oil content are based on different working principles, the application of each method is not the same (Bordenave, 1993; Xue et al., 2016) (Fig. 1). For example, the fraction extracted by chloroform looks more like crude oil (Dembicki, 2016; Wang, 2014), and both petroleum hydrocarbons and NSO compounds are measured. However, due to the volatilization of chloroform during chloroform extraction, the light hydrocarbons (C_6–C_{13}) with strong mobility in crude oil are completely lost (Xue et al., 2016). Volatile hydrocarbons (S_1) includes part of the petroleum hydrocarbons in shale oil and has a low carbon number due to the hydrocarbons emitted by rock samples heated to temperatures not higher than 300 °C (the boiling point of n-C_{17} is 302 °C and that of n-C_{18} is 316 °C) (Behar et al., 2001; Horsfield, 1984). Therefore, using these methods, the parameters of total oil content represented by chloroform extraction and volatile hydrocarbons (S_1) are underestimated. It has been observed that the higher the oil content and mobility, the higher the shale oil production (Lu et al., 2016). For the above reasons, a conceptual model of this method has been proposed, as follows:

$$OCEI = w_1 \times LI + w_2 \times GI + w_3 \times CI \tag{1}$$

where *OCEI* is the oil content evaluation index, *LI* is the normalized oil content evaluation index-related liquid components, *GI* is the normalized oil content evaluation index-related gas components, *CI* is the normalized oil content evaluation index-related core description, and w_1, w_2 and w_3 are the relative weights of the evaluation index *LI*, *GI* and *CI*. These normalized indexes are defined as:

$$LI = \frac{LI^* - LI^*_{\min}}{LI^*_{\max} - LI^*_{\min}} \tag{2}$$

$$GI = \frac{GI^* - GI^*_{\min}}{GI^*_{max} - GI^*_{\min}} \tag{3}$$

$$CI = \frac{CI^* - CI^*_{\min}}{CI^*_{\max} - CI^*_{\min}} \tag{4}$$

where LI^*, GI^* and CI^* are the oil content evaluation indexes through depth, $LI^*_{\min}$ and $LI^*_{\max}$ are the minimum and maximum values of the evaluation index (LI^*) for the investigated formation, $GI^*_{\min}$ and $GI^*_{\max}$ are the minimum and maximum values of the evaluation index (GI^*) for the investigated formation, $CI^*_{\min}$ and $CI^*_{\max}$ are the minimum and maximum values of the evaluation index (CI^*) for the investigated formation. $LI^*_{\min}$, $LI^*_{\max}$, $GI^*_{\min}$, $GI^*_{\max}$, $CI^*_{\min}$ and $CI^*_{\max}$ are constants, and LI^*, GI^* and CI^* are variables that depend on depth.

Previous studies have found that the content of liquid and gaseous hydrocarbons plays an important role in the exploration and development of shale oil (Lu et al., 2016). Therefore, in this paper, methods for evaluating liquid and gaseous hydrocarbons have been established. Through establishing a mathematical model, the evaluation index *LI*, which is associated with the liquid hydrocarbon segment, is created in

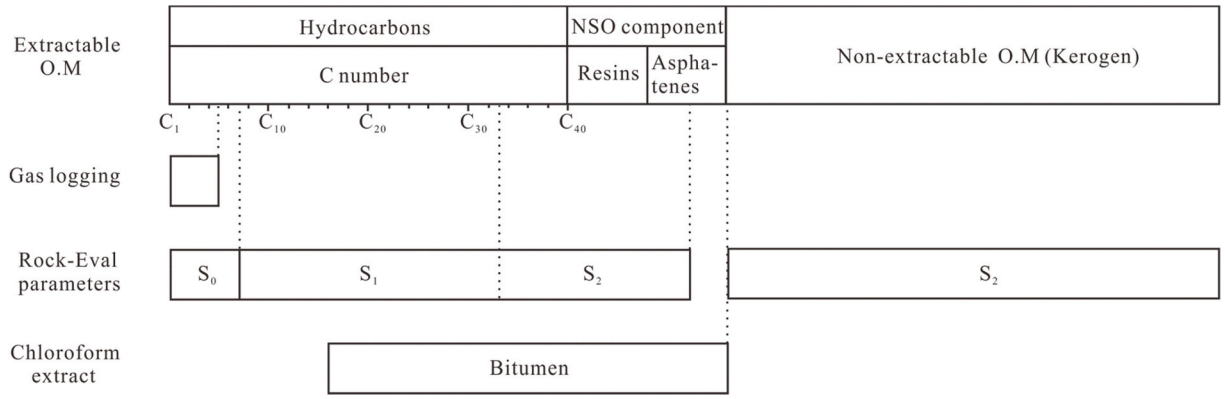

Fig. 1. Comparison of analysis objectives among various methods (revised from Bordenave et al., 1993).

combination with the oil saturation logging, crude oil density, porosity logging and density logging. The indicator is then calibrated with volatile hydrocarbon and chloroform extraction data. When the formation develops a large number of fractures, this parameter will be affected to some extent. Considering this factor, a relatively accurate evaluation index, *LI* + *CI*, related to liquid hydrocarbon is proposed and is combined with the quantitative description of core oil content. The evaluation index *GI*, which is related to the gaseous hydrocarbon segment, is derived from gas logging data. The threshold value of the OCEI is determined by the shale oil production of several commercial oil wells under existing technical conditions. The specific workflow is shown in Fig. 2.

3. Geological setting

The Jimusaer Sag is a secondary structural unit along the southeastern margin of the Junggar Basin and has an area of approximately 1300 km^2 (Fig. 3a). The sag is bordered by the Jimusaer and Laozhuangwan faults to the north, the Santai and Houbaozi faults to the south, and the Xidi fault to the west and pinches out to the eastern Guxi uplift (Cao et al., 2017; Liu et al., 2019a,b; Qiu et al., 2016a,b; Wu et al., 2016) (Fig. 3b). It is a west-inclined dustpan-shaped depression developed on Middle Carboniferous basement (Fig. 4). The sag has undergone multiple tectonic movements, including Hercynian, Indosinian, Yanshan and Himalayan, but its internal structure is stable and gentle (Luo et al., 2007; Xiao et al., 2008). From base to top, it is filled with Permian to Quaternary sedimentary sequences, with the maximum thickness exceeding 5000 m in the west (Fig. 3c). In general, the thickness of the strata from Permian to Cretaceous shows a trend of gradual thinning to the east.

Three stratigraphic units, from bottom to top, were developed in the Permian, namely, the Middle Permian Jingjingzigou Formation, the Lucaogou Formation and the Upper Permian Wutonggou Formation. Among them, the Lucaogou Formation is one of the important oil-bearing stratigraphic formations in the eastern part of the Junggar Basin. It is spread throughout the sag, revealing a trend of thickening

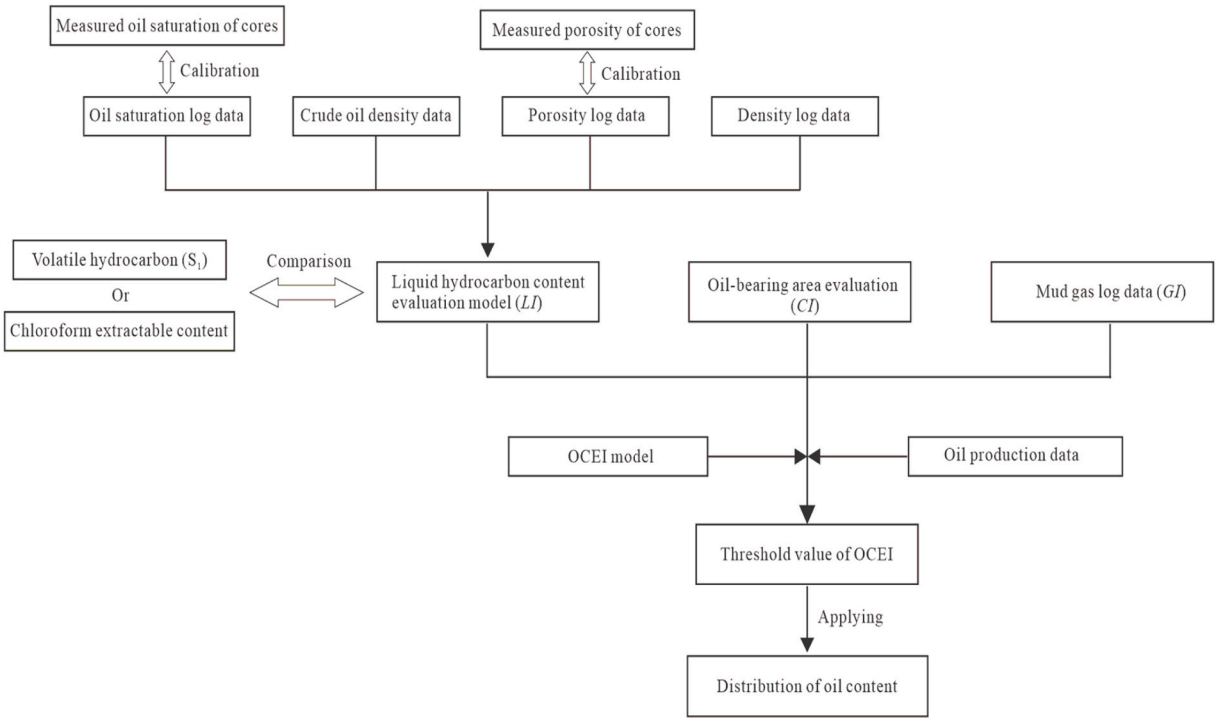

Fig. 2. Workflow chart for the evaluation of oil content in shale oil systems. *LI* = the normalized oil content evaluation index-related liquid components; *GI* = the normalized oil content evaluation index-related gas components; *CI* = the normalized oil content evaluation index-related core description; OCEI = oil content evaluation index.

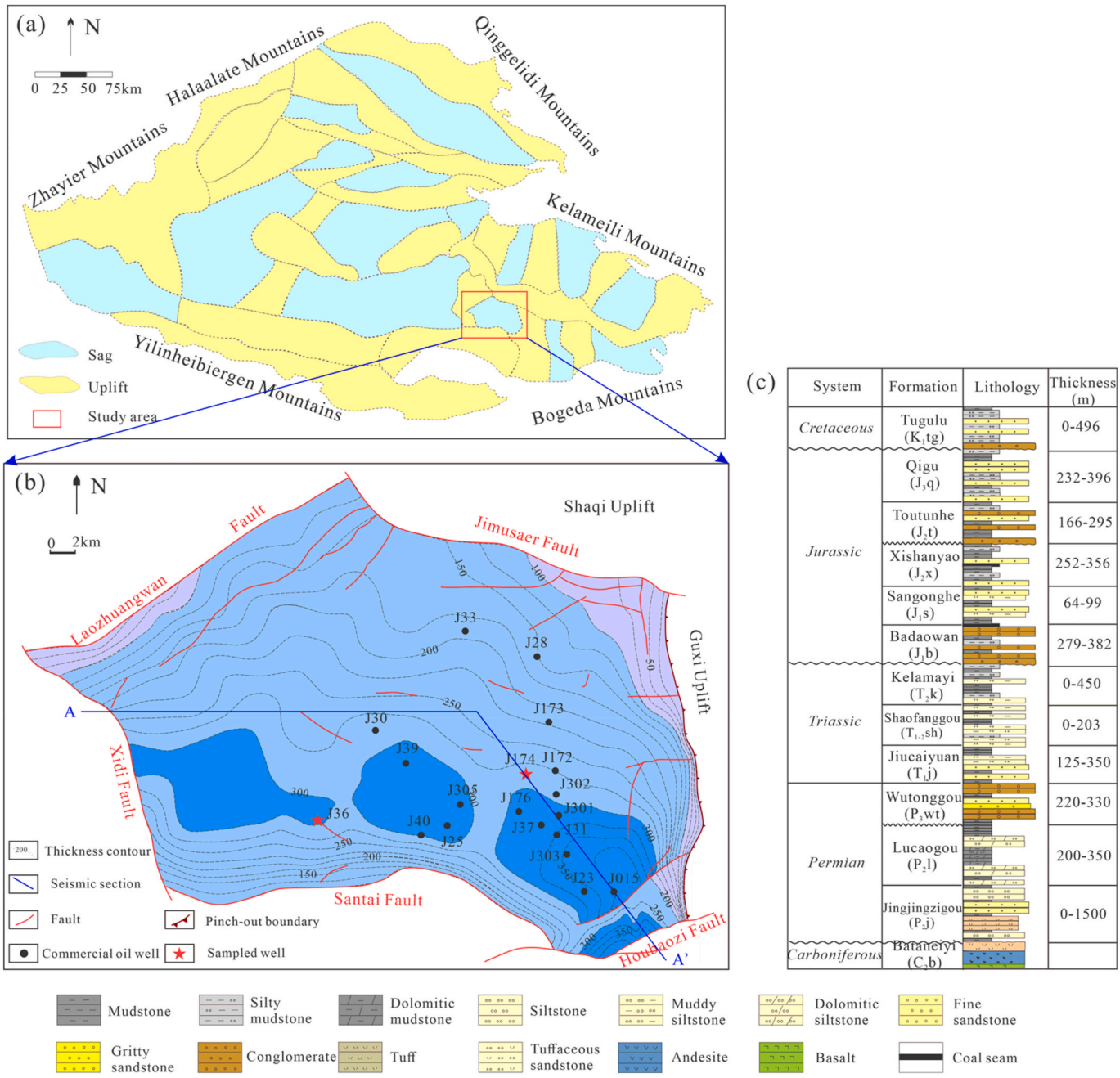

Fig. 3. Location and stratigraphic framework of the Jimusaer Sag. (a) The geographic location of the Jimusaer Sag in the Junggar Basin; (b) structural framework and thickness contour map of the Lucaogou Formation in the Jimusaer Sag; (c) stratigraphic column of this region (revised from Qiu et al., 2016 and Wu et al., 2016).

towards the west and north, with an average thickness of approximately 200–350 m. The formation was deposited in a saline lacustrine environment during the Middle Permian (Cao et al., 2016; Kuang et al., 2013; Wang et al., 2007). It is dominated by organic-rich mudstones that are either interbedded with or vertically adjacent to organic-lean rocks including carbonates, siltstone, pyroclastics, and others. According to the characteristics of its logging curves and maximum flooding surface, the Lucaogou Formation is vertically divided into two members, the lower section (P_2l_1) and the upper section (P_2l_2) (Zhang et al., 2019). Commercial oil flow has been obtained from the sweet spots in these shale-oil systems through several wells, including the wells J172, J25 and J174. Among these wells, the horizontal well J172 has produced for nearly 1800 days and has a cumulative oil production of nearly 1.9×10^4 tons (Wu et al., 2019). Currently, it is in a stage of stable production, with a daily oil production of approximately 4 tons. Due to its rich oil and gas resources and its huge exploration potential, shale oil in Jimusaer Sag has attracted increasing attention.

4. Samples and analyses

A series of 292 core samples from the Lucaogou Formation were collected from well J174 in the eastern part of the Jimusaer Sag (Fig. 3b). These samples were subjected to Rock-Eval pyrolysis to determine the total organic carbon (TOC) and volatile hydrocarbon (S_1) content. These samples were powdered to 200 mesh grain size. For TOC analyses, each 100-mg sample was treated in a clean crucible with hydrochloric acid to remove carbonates; it was then washed with deionized water, which was exchanged every half hour, for 2 days. These samples were subsequently dried, and the residual organic carbon content was determined using a Leco CS400 analyzer (Peters, 1986). A

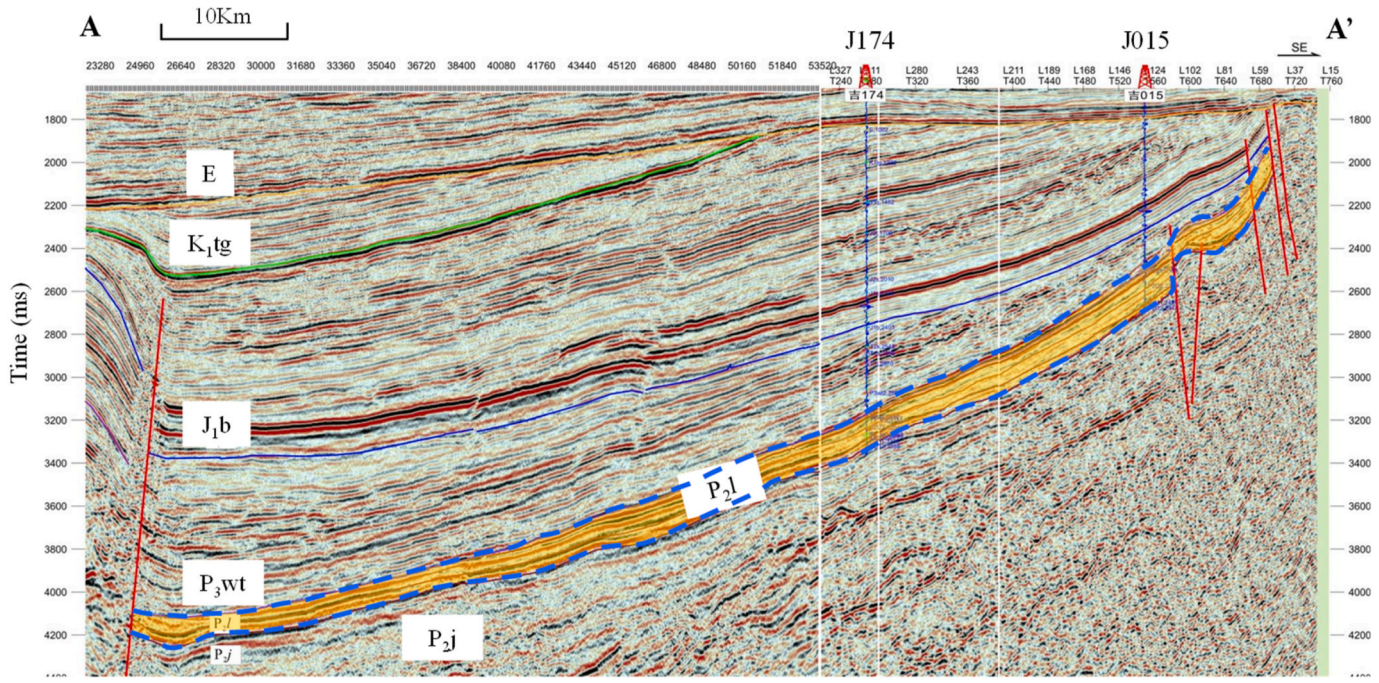

Fig. 4. Seismic profile showing the stratigraphic architecture in the Jimusaer Sag. The location of the seismic profile is shown by line AA′ in Fig. 3(b). The Lucaogou Formation (P_2l) is located between the blue dotted lines. (For interpretation of the references to color in this figure legend, the reader is referred to the Web version of this article.)

Rock-Eval 6 instrument was used for pyrolysis analysis. The temperature was initially set at 300 °C for 3 min, and the sample was then heated to 600 °C at a rate of 50 °C/min. The pyrolysis parameters, including S_1, S_2 and T_{max}, were obtained (Espitalié et al., 1977, 1984). Ninety-two lacustrine shale samples from the Lucaogou Formation in the Jimusaer Sag were used to determine extractable content. These powder samples were extracted in a Soxhlet apparatus with a dichloromethane/methanol mixture (93:7) for 72 h. Thirty-six core plugs were used for total porosity determination, and twelve core plugs were used for oil saturation determination. Oil saturation and total porosity were measured by atmospheric distillation and by the helium porosimeter method, which follows the Chinese Oil and Gas Industry Standard GB/T 34906-2017 of P.R. China (National Standard of practices for core analysis, 2017). Standard cylindrical core plugs one inch in diameter were first subjected to high-temperature dry distillation in a dry distillation cylinder. After all the water in the samples had been distilled, the water vapor was dissolved in anhydrous ethanol, and the volume of water was measured using a micromoisture meter. The core plugs were washed, dried, and weighed and the total porosity was measured using a helium porosimeter, thereby obtaining water or oil saturation by mathematical formula calculation (Wang et al., 2014). The experimental analysis data of this study was provided by the Experimental Center of Exploration and Development Research Institute of PetroChina Xinjiang Oilfield Company.

5. Procedures and results for oil content evaluation

5.1. Evaluation index LI*

5.1.1. Porosity logging evaluation and calibration

The Wyllie equation was adopted for porosity prediction in the intervals of interest because of its simplicity and convenience (Castagna et al., 1993; Raymer et al., 1980; Wyllie et al., 1956). However, the accuracy of traditional porosity prediction methods is generally affected by the heterogeneity of lithology, and this may result in difficulties in realizing the desired goals. To minimize such errors, an improved porosity prediction method is used for porosity evaluation. The final porosity of the target interval is obtained from the arithmetic mean value of the porosity evaluated by acoustic logging and density logging. The equation can be expressed as

$$\varphi_D = \frac{\rho_{ma} - \rho_b}{\rho_{ma} - \rho_f} \tag{5}$$

$$\varphi_A = \frac{\Delta t_b - \Delta t_{ma}}{\Delta t_f - \Delta t_{ma}} \tag{6}$$

$$\varphi = \frac{\varphi_D + \varphi_A}{2} \tag{7}$$

where φ is the final porosity of the target interval (in %), φ_D and φ_A are the predicted porosity values from the density and acoustic logging (in %), ρ_b and Δt_b are the values from the density and the acoustic logging through depth (in g/cm^3 and μs/ft, respectively), ρ_{ma} and Δt_{ma} are the values from the density and acoustic logging in the matrix (in g/cm^3 and μs/ft, respectively), and ρ_f and Δt_f are the values from the density and acoustic logging of the fluid of the pores (in g/cm^3 and μs/ft, respectively).

Based on the above model, continuous porosity values of the target interval can be determined. The accuracy of this method is verified by comparing the predicted porosity with the measured porosity. Fig. 5a shows a comparison of the core porosity and the predicted porosity in well J174. The correlation coefficient (R^2) is 0.871, indicating that the porosity prediction method is suitable for predicting the porosity.

5.1.2. Oil saturation logging evaluation and calibration

Reservoir evaluation is one of the important tasks in oil and gas field exploration and development. In this regard, it is important to determine specific rock properties, such as water saturation. Accurate prediction of the water saturation of the intervals of interest is essential to reduce the risks of exploration and development of oil and gas fields. Archie's equation is used in most cases to calculate water saturation (Archie, 1942). In this study, this method is adopted to evaluate the water saturation of the Lucaogou Formation. The equation is expressed as

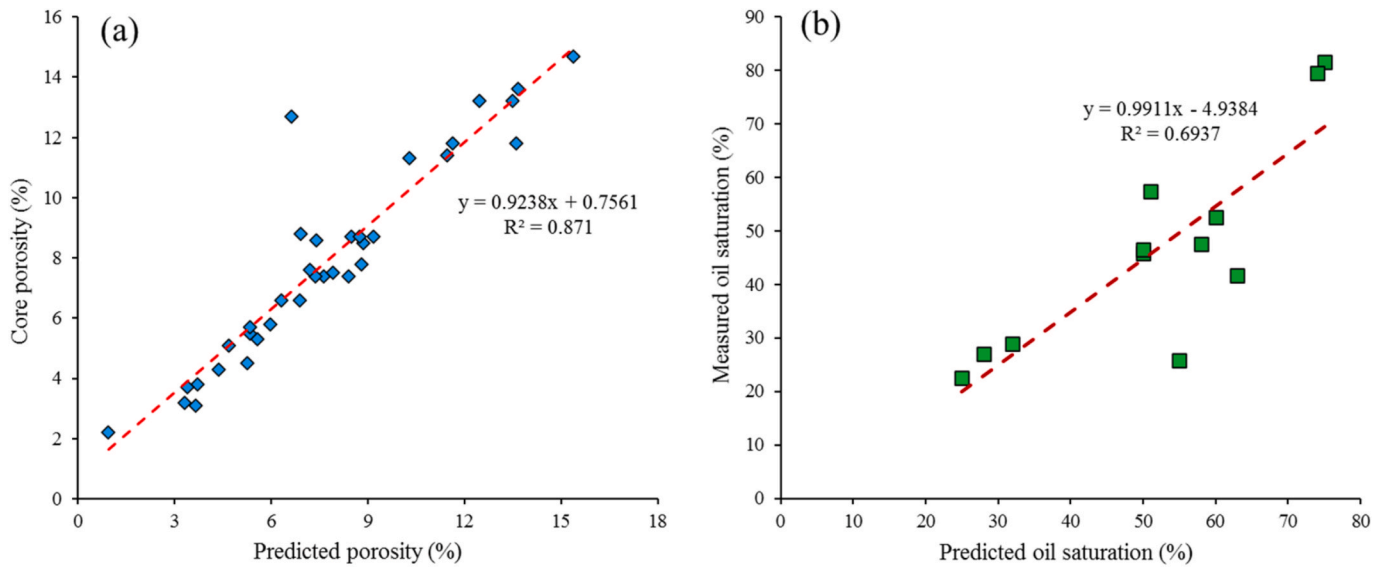

Fig. 5. (a) Crossplot of predicted porosity and core porosity. (b) Crossplot of predicted oil saturation and measured oil saturation. R refers to the correlation coefficient.

$$R_t = \frac{aR_w}{\varphi^m S_w^n} \tag{8}$$

where R_t is the true formation resistivity in Ωm, R_w is the formation water resistivity in Ωm, φ is the final porosity of the target interval in %, S_w is the water saturation in %, a is a proportional coefficient, m is the cementation exponent and n is the saturation index (Jin et al., 2020; Qin et al., 2016).

The accuracy of parameters a, m and n in Archie's equation affects the accuracy of the water saturation calculation. Over the years, extensive efforts have been made to determine these parameters. Based on the analysis of rock samples from well J174, a is taken to be equal to 0.98, m is taken to be equal to 1.73, and n is taken to be equal to 1.76. On the basis of the above model, the oil saturation prediction curve of the target interval in well J174 is established. As shown in Fig. 5b, the predicted values of oil saturation have a good linear relationship with the measured values of the samples; the linear coefficient is approximately equal to 1, and the correlation coefficient (R) is greater than 0.8. This indicates that the oil saturation evaluation model can be applied to other wells.

5.1.3. Indicator LI* model and calibration

A few indicators, such as So, S_1 and extraction content, are available for characterization of the liquid hydrocarbon content of shale-oil systems. Although there are multiple parameters for characterization, there are differences in their geological meanings. The oil saturation (S_o) refers to the percentage of liquid hydrocarbons per unit volume of rock pores (Espitalié et al., 1984). The pyrolysis parameter S_1 and the extractable content represent the percentage of liquid hydrocarbons per unit mass of rock (Espitalié et al., 1984). Due to the low content of resins and asphaltenes in lacustrine crude oil, the pyrolysis parameter S_1 and extractable content tend to show a good linear relationship (Fig. 6). These two parameters are important for evaluating shale oil resources, but it is difficult to obtain all geological parameters unless the core samples are complete.

Based on the above, the indicator LI^* can be established and used to evaluate the liquid hydrocarbon content using combined data from oil saturation, porosity and density loggings and crude oil density. The measurement. LI^* is calculated as

$$LI^* = \frac{m_{HC}}{m_{Rock}} \times 100\%$$

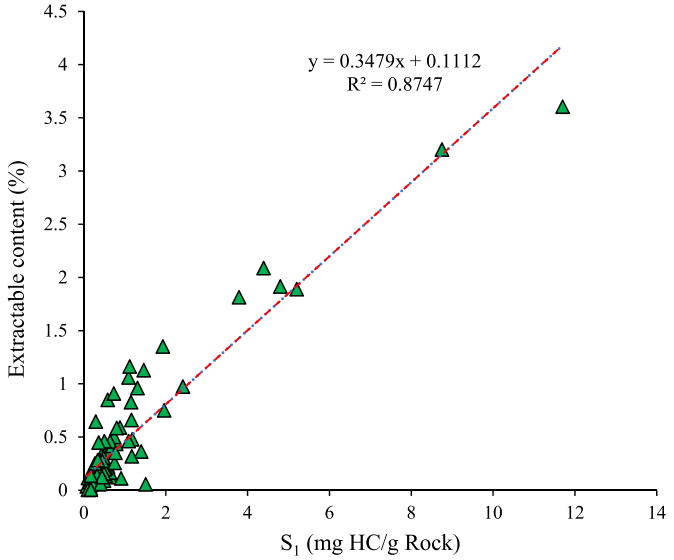

Fig. 6. Relationship between volatile hydrocarbon (S_1) and chloroform extractable content. R refers to the correlation coefficient.

$$= \frac{\rho_{HC} \times V_{HC}}{\rho_b \times V_b} \times 100\%$$

$$= \frac{V_{HC}}{V_{Por}} \times \frac{V_{Por}}{V_b} \times \frac{\rho_{HC}}{\rho_b} \times 100\%$$

$$= S_o \times \varphi \times \frac{\rho_{HC}}{\rho_b} \times 100\% \tag{9}$$

where LI^* is the liquid hydrocarbon content through depth (in %), m_{HC} and m_{Rock} refer to the masses of liquid hydrocarbons and rocks, respectively (in g), ρ_{HC} and ρ_b refer to the densities of liquid hydrocarbons and rocks, respectively (in g/cm^3), V_{HC}, V_{Por}, and V_b refer to the volumes of liquid hydrocarbons, pores, and rocks, respectively (in cm^3), S_o is the oil saturation (in %), and φ is the final porosity of the target interval (in %).

The physical meaning of equation (9) is the content of liquid

hydrocarbons in the rock per unit mass. Using the above model, the quantitative evaluation of liquid hydrocarbon content in the shale oil systems can be achieved, and the evaluation can be transformed from discrete data evaluation to continuous logging data evaluation. Besides, these conventional logging curves are also easy to obtain. The shale oils produced from the Lucaogou Formation by the eleven wells in the Jimusaer Sag show no significant differences in density (Table 1). As shown in Table 1, the density of upper section crude oil varies from 0.881 to 0.896 g/cm^3, while the density of lower section crude oil ranges from 0.901 to 0.922 g/cm^3. Based on analysis of the available samples, ρ_b takes the average density of all samples, namely, 0.90 g/cm^3. To further verify the effectiveness of this method, the liquid hydrocarbon content calculated by the method is compared with the pyrolysis parameter S_1 and with the extractable content. Fig. 7 shows that there is a consistent variation tendency between the *LI** indicator and the pyrolysis parameter S_1 and the extractable content. However, it can also be observed that some data points deviate from this trend. The reason for this may be that a large number of fractures developed in some intervals. Besides, according to the theoretical derivation process of this formula, this method is more suitable for characterizing the liquid hydrocarbon content in porous media. On the whole, the index *LI** can effectively reflects the variation in the liquid hydrocarbon content in the target intervals.

5.2. Evaluation index CI*

Cores not only provide a detailed interpretation of stratigraphic variation and developmental characteristics but also information on oil and gas migration (Gardner et al., 2003; Shanmugam et al., 1995; Tesson et al., 2000). The observation of core samples from well J174 reveals that the oil-bearing properties of different strata are highly heterogeneous (Fig. 8). According to the characteristics of the oil-bearing area, oil-bearing fullness and drip test, the oil-bearing degree of the core is divided into 7 different levels (National Standard of practices for core analysis, 2017). To facilitate geostatistical analysis, these levels are further assigned to different ordered values for which higher values indicate higher oil content. These levels are: Level 6 (oil full): the oil-bearing area is over 95% and is full of oil; Level 5 (oil rich): the oil-bearing area is more than 75%, and the oil distribution is uniform; Level 4 (oil stained): the oil-bearing area exceeds 40%, and the oil distribution is patchy; Level 3 (oil spot): the oil-bearing area is between 5% and 40% and presents a spotted and banded distribution; Level 2 (oil trace): the oil-bearing area is less than 5% and shows a scattered pattern of spots; Level 1 (fluorescence): the oil-bearing area is invisible but can be detected by fluorescence; Level 0 (no fluorescence): the oil-bearing area is invisible and cannot be detected by fluorescence. Based on the above grading evaluation criteria, the quantitative characterization of oil content in core samples can be achieved.

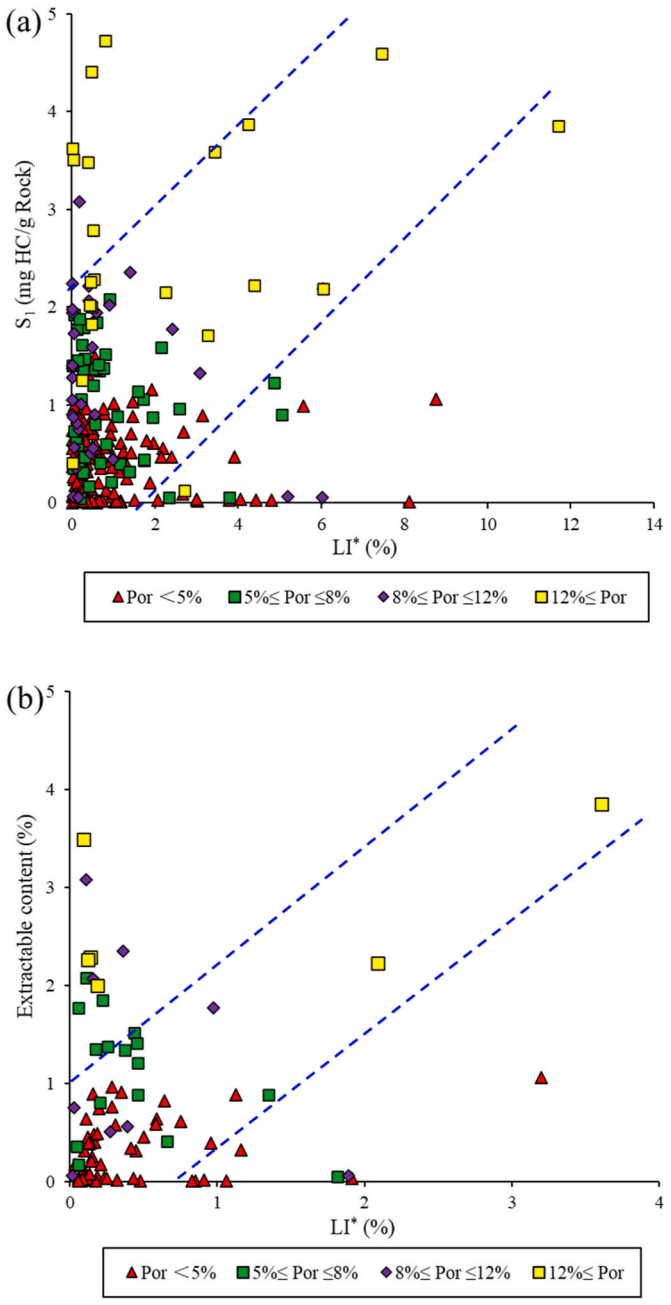

Fig. 7. (a) Relationship between LI* and the pyrolysis parameter S_1. (b) Relationship between LI* and chloroform extractable content.

Table 1
Comparison of the density of shale oils obtained from different wells.

Well	Number of samples	Depth (m)	Formation	Section	Density (g/cm^3)	Viscosity (50 °C mPa s)	Freezing point (°C)
J171	6	3074.0 ~ 3102.5	P_2l_2	Upper	0.889	45.65	12.5
J172	2	2920.0 ~ 2970.0	P_2l_2	Upper	0.885	58.80	32.0
J172_H	5	3150.92 ~ 4360.0	P_2l_2	Upper	0.896	73.36	22.6
J23	3	2309.0 ~ 2385.0	P_2l_2	Upper	0.881	133.16	35.8
J25	2	3403.0 ~ 3425.0	P_2l_2	Upper	0.895	76.03	21.2
J173	7	3088.0 ~ 3109.0	P_2l_2	Upper	0.883	53.72	25.0
J174	10	3255.0 ~ 3314.0	P_2l_1	Lower	0.922	434.92	0.4
J31	2	2875.0 ~ 2945.0	P_2l_1	Lower	0.917	342.35	5.5
J33	5	3664.0 ~ 3717.0	P_2l_1	Lower	0.909	167.28	9.0
J251_H	8	4414.5 ~ 4960.0	P_2l_1	Lower	0.901	103.70	9.1
J36	3	4209.0 ~ 4255.0	P_2l_1	Lower	0.903	105.37	8.7

Abbreviations: P_2l_1 refers to the lower Lucaogou Formation; P_2l_2 refers to the upper Lucaogou Formation.

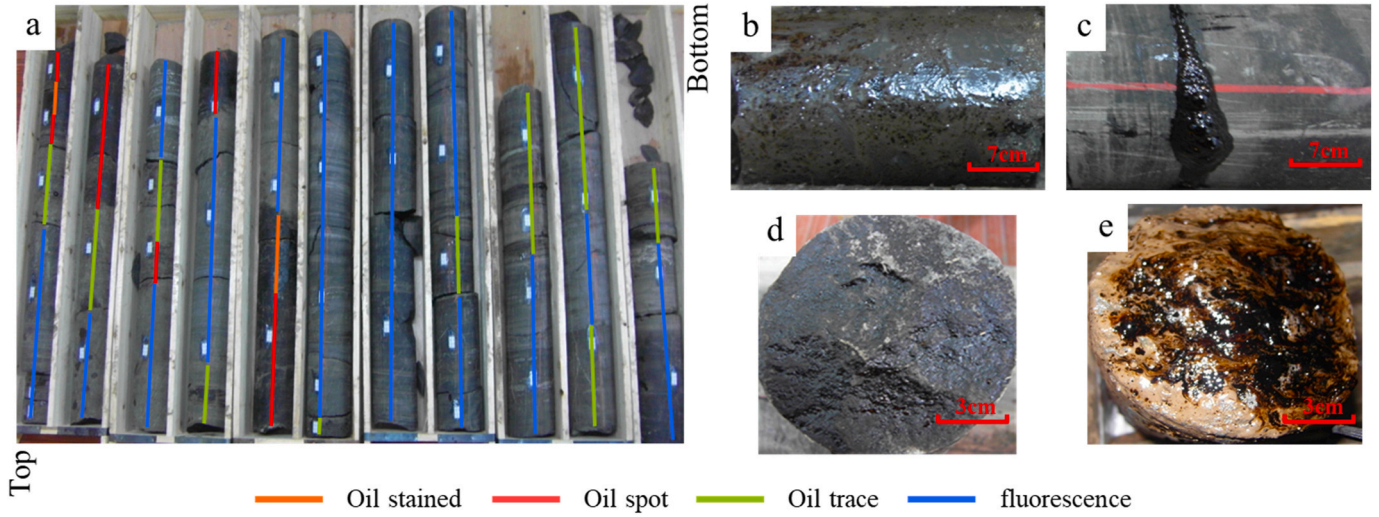

Fig. 8. Core photos showing the oil-bearing properties of well J174 in the Lucaogou Formation. (a) Observation of the oil-bearing properties in core samples of well J174 from 3275.36 m to 3284.30 m. (b) Oil spot. (c) Oil trace. (d) Oil spot. (e) Oil stained.

5.3. Evaluation index GI*

Compared with the marine shale oil successfully developed in North America, the continental shale oil in China is characterized by its lower maturity (Ro = 0.5–1.1%) and poorer mobility (GOR = 20–60 m^3/m^3) (W. Zhao et al., 2020). An increase in the amount of dissolved gas increases the mobility of the crude oil. Due to their low boiling point, light hydrocarbons are easily lost during sample storage and experimental analysis. Many methods for the recovery of light hydrocarbons, including the chromatography method, pyrolysis combined with extraction, chemical kinetic theory, pressure coring and other methods, are presently available (Jiang et al., 2016; Li et al., 2020; Wang et al., 2014; Zhu et al., 2015). In this study, we used mud gas logging to assess the light hydrocarbon content under actual geological conditions. With the development of flame ionization detectors, mud gas logging systems can provide a reliable analysis of C_1–C_5 hydrocarbons. Therefore, this method compensates for the shortcomings of the above methods. Based on the total gas concentration, some researchers have established corresponding classification standards (Dembicki, 2016; Hammerschmidt et al., 2014; Noble, 1991). Noble (1991) provides some grading criteria for total gas (C_1–C_5) concentration expressed in ppm. A total gas concentration lower than 100 ppm is considered background, while total gas concentrations of 1000–10000 ppm suggest rich source rocks, and values higher than 10000 ppm indicate excellent source rocks (Dembicki, 2016).

5.4. Estimating the relative weight of variables

For blocks with a high degree of exploration and some commercial oil wells, the actual production of shale oil is a direct indicator for evaluating oil content. Based on the correlation between the shale oil productivity (daily oil production per meter, $t/d{\cdot}m^{-1}$) and these evaluation indexes during the stable production stage, the weight coefficients assigned to the three evaluation parameters are determined. The higher the correlation between a certain evaluation parameter and the oil production, the greater the influence of this variable on the oil production, the greater the weight value assigned. There are several common methods for weight determination, such as data envelopment analysis (DEA), analytical hierarchy process (AHP), simple additive weighting (SAW), grey relational analysis and so on (Çaydaş and Hasçalık, 2008; Kolahan et al., 2011; Kuo et al., 2008; Tosun, 2005; Yang et al., 2007; Yang and Hung, 2007; Zeng et al., 2007). In this study, we applied the grey relational analysis method to determine the respective weights of the evaluation indicators *LI*, *CI* and *GI*. The grey theory first proposed by Deng (1982) has been successfully applied to various research fields (Asokan et al., 2007; Lin et al., 2006). It has been proven to be an effective means to analyze the uncertain relationship between the reference sequence and every comparability sequence (Asokan et al., 2007; Tosun, 2005). The primary scenarios of the algorithm can be described as follows: Let X_0 be the reference sequence with m entities. Then:

$$X_0 = \{x_0(1), x_0(2), \ldots, x_0(\mathrm{m})\} \tag{10}$$

where m is the number of parameters.

Let X_i be the comparability sequence with m entities (the number of experimental data items). Then:

$$X_i = \{x_i(1), x_i(2), \ldots, x_i(\mathrm{m})\}, \quad i = 1, 2, \ldots n. \tag{11}$$

where n is the number of experimental data items.

Normalize the sequences to eliminate the influence of adopting different units, and the normalized sequences can be expressed as:

$$x_i^*(j) = \frac{x_i(j) - \min x_i(j)}{\max x_i(j) - \min x_i(j)} \tag{12}$$

where max $x_i(j)$ is the maximum value of entity j, and min $x_i(j)$ is the minimum value of entity j. After the data is normalized, the grey relational coefficient is calculated to express the relationship between the reference sequence and the compared sequence. The formula is as follows:

$$\gamma_{oi}(j) = \frac{\Delta\min + \rho\Delta\max}{\Delta_{0i}(j) + \rho\Delta\max} \tag{13}$$

where Δ_{0i}(j) is the absolute difference between the reference sequence ($x_0^*(j)$) and the comparability sequence ($x_i^*(j)$), namely $\Delta_{oi}(j) = |x_0^*(j) - x_i^*(j)|$; $\Delta\min = \min_i \min_j |x_0^*(j) - x_i^*(j)|$ and $\Delta\max = \max_i \max_j |x_0^*(j) - x_i^*(j)|$ are the minimum and maximum value of the difference between $x_0^*(j)$ and $x_i^*(j)$. ρ is the identification or distinguishing coefficient which is defined in the range $0 \leq \rho \leq 1$. $\rho = 0.5$ is generally adopted.

After obtaining the grey correlation coefficient, the average value of the grey correlation coefficient is usually taken as the grey relational grade. It is calculated as follows:

$$\xi_i = \frac{1}{n}\sum_{j=1}^{n} \gamma_{0i}(j) \tag{14}$$

Then, the relative weight of variables is defined as

$$w_i = \xi_i \Big/ \sum_{i=1}^{n} \xi_i \quad (15)$$

where w_i is the weight coefficient of the i-th variable.

The production data of 12 wells are used to establish the relative weights of various geological parameters (*LI*, *CI* and *GI*). The detailed characteristics of these commercial wells are shown in Table 2. Equation (12) is used to normalize the oil productivity, *LI**, *CI** and *GI**. Using Equation (13), we can calculate the grey relational coefficient of these evaluation indexes, as shown in Table 3. Also, the average value of the grey correlation coefficient is computed according to Equation (14). It can be found from Table 3 and Fig. 9 that the grey correlation coefficient of the evaluation index *LI** is relatively the largest, indicating that this index is a key indicator for shale oil production prediction. Based on Equation (15), we can obtain the relative weight of each variable. The weights of the evaluation indicators *LI**, *CI** and *GI** are 0.38, 0.31 and 0.31 respectively (Table 3).

5.5. Threshold value of the OCEI

Based on the above model, the oil content evaluation of shale oil of various compositions can be accomplished. The shale oil production data and OCEI data from the 12 wells (Table 2) of the Lucaogou Formation test section in the Jimusaer Sag have been analyzed, as shown in Fig. 10.The shale oil productivity increases with increasing OCEI, and there is a critical point. When the value of OCEI is less than 0.39, the production of shale oil is less than 0, indicating that it cannot obtain commercial oil under the current technical conditions. When the value of OCEI is higher than 0.39, shale oil production increases rapidly. Therefore, we assign 0.39 as the threshold value of the OCEI for the potential favorable development zones in the Jimusaer Sag. When the OCEI value of a certain interval is greater than 0.39, then this interval is a favorable pay zone.

6. Cases and discussion

The following sections use core and well logging data from wells J174 and J36 in the Jimusaer Sag to determine favorable pay zones through the OCEI method. These examples in this study are combined with actual oil production and compared with the hydrocarbon expulsion threshold method proposed by Jarvie (2012). In this way, the effectiveness of the OCEI method in selecting favorable intervals of shale oil is demonstrated.

6.1. Well J174

Well J174, which was systematically cored from 3046.2 m to 3442.2 m (9994.1–11293.3 ft), including the Lucaogou Formation, is a typical well that has been used in shale oil systems research in the Jimusaer Sag and provides basic data for the exploration and development of lacustrine shale oil in China. Thermal maturity, as indicated by T_{max}, suggests that the organic matter shown in Fig. 11 is in the main stage of hydrocarbon generation. Given this level of thermal maturity, the present-day hydrogen index values of the $P_2l_1^2$ and $P_2l_2^2$ intervals are significantly higher than those of the other intervals, indicating that the organic matter in these two intervals has a greater oil-generating potential. Formation testing of the interval from 3116 m to 3146 m (10223.1–10321.5 ft) produced 2.15 tons of oil per day, while formation testing conducted between 3255 m and 3314 m (10679.1–10872.7 ft) yielded 7.76 tons of oil per day (Table 2).

The vertical distribution of oil saturation, porosity, *LI**, *GI** and *OCEI* is predicted in the Lucaogou Formation of well J174 using conventional logging curves, as shown in Fig. 11. The logging evaluation results for porosity and oil saturation are very consistent with the measured values (solid points) (Fig. 11 and Table 4), indicating that the porosity and oil saturation logging evaluation models are reliable and can be applied to other wells. It can be observed that the porosity and oil saturation exhibit strong vertical heterogeneity. Based on the indicators *LI**, *GI** and *CI**, the vertical distribution of OCEI is shown; in the figure, the left boundary of the track OCEI is set to 0.39, and the intervals with the OCEI greater than 0.39 are filled with a red color. Track potential target1 shows the favorable reservoir intervals determined by the OCEI method proposed in this study. Track potential target2 shows the favorable reservoir intervals determined by the hydrocarbon expulsion threshold proposed by Jarvie (2012) using the value of S_1/TOC.

There is a small amount of depth interval with the OCEI greater than 0.39 in the Lucaogou Formation of well J174. There exists an OCEI peak at the interval from 3275.1 to 3279.2 m (10742.33–10755.78 ft). This peak is within the range of oil testing interval from 3255 m to 3314 m (10679.1–10872.7) (the area surrounded by the pink box in Fig. 11). Using the hydrocarbon expulsion threshold based on the combination of S_1 and TOC indicates that the intervals from 3254.85 to 3297.81 m (10675.91–10816.82 ft) and from 3315.75 to 3336.95 m (10875.99–10945.2 ft) are potentially favorable intervals, findings that are basically consistent with the results of the OCEI method proposed in this article. In addition, another interval from 3113.12 to 3131.60 m (10211.03–10271.65 ft) can also be a potentially favorable interval. The oil testing result in this interval is 2.15 tons per day, which provides sufficient evidence for testing the OCEI method to predict shale oil pay

Table 2
Characteristics of the testing oil intervals of commercial wells in the Jimusaer Sag. Oil productivity is the result of the daily output divided by the thickness of reservoirs; *LI** = the oil content evaluation index-related liquid components; *CI** = the oil content evaluation index-related core description; *GI** = the oil content evaluation index-related gas components. The evaluation indexes *LI**, *CI** and *GI** in Table 2 are the average values in the testing oil intervals.

Number of samples	Well name	Interval	Oil test section (m)	Oil rate (t/d)	Thickness of reservoir	Oil productivity (t/d·m)	*LI** (%)	*CI**	*GI** (ppm)
1	J174	P_2l_2	3116–3146	2.15	18.9	0.114	2.21	896	1.68
2		P_2l_1	3255–3314	7.76	34.8	0.223	1.61	2170	1.47
3	J25	P_2l_2	3403–3425	18.25	20.5	0.890	2.66	3007	1.55
4	J36	P_2l_1	4209–4255	13.88	32.7	0.424	1.84	10706	1.88
5	J31	P_2l_2	2707–2746	2.79	32.3	0.086	1.48	3350	2.60
6		P_2l_1	2875–2945	0.71	51.13	0.014	1.30	5351	2.34
7	J37	P_2l_2	2830–2849	6.31	17.15	0.370	2.93	3406	3.56
8	J23	P_2l_2	2309–2385	0.24	71.38	0.003	1.33	1425	1.97
9	J301	P_2l_2	2762–2776	9.53	13.42	0.710	2.46	3897	3.23
10	J303	P_2l_2	2580–2595	4.48	9.44	0.470	2.34	2635	3.12
11		P_2l_2	2598–2604	4.69	6.01	0.780	3.29	2597	2.98
12	J30	P_2l_2+P_2l_1	4018–4184	10.54	89.94	0.120	1.58	2525	1.19
13	J172	P_2l_2	2920–2970	3.26	13.13	0.250	2.09	729	2.44
14	J33	P_2l_1	3664–3717	5.51	17.13	0.320	1.40	5029	1.64
15	J176	P_2l_2	3028–3063	5.27	20.5	0.260	2.16	1102	2.28

Abbreviations: P_2l_1 refers to the lower Lucaogou Formation; P_2l_2 refers to the upper Lucaogou Formation.

Table 3
Grey relational coefficient and relative weight of these evaluation indexes.

Number of samples	Normalized values for oil productivity	Normalized values for *LI**	Normalized values for *CI**	Normalized values for *GI**	GRC values for *LI**	GRC values for *CI**	GRC values for *GI**
1	0.125	0.46	0.02	0.21	0.5653	0.8035	0.8452
2	0.248	0.16	0.14	0.12	0.8278	0.8100	0.7715
3	1.000	0.68	0.23	0.15	0.5773	0.3576	0.3361
4	0.475	0.27	1.00	0.29	0.6810	0.4506	0.7032
5	0.094	0.09	0.26	0.59	1	0.7214	0.4623
6	0.012	0.00	0.46	0.49	0.9800	0.4887	0.4767
7	0.414	0.82	0.27	1.00	0.5156	0.7508	0.4232
8	0.000	0.02	0.07	0.33	0.9737	0.8659	0.5677
9	0.797	0.58	0.32	0.86	0.6700	0.4732	0.8767
10	0.526	0.52	0.19	0.81	0.9992	0.5630	0.6006
11	0.876	1.00	0.19	0.76	0.7802	0.3843	0.7849
12	0.132	0.14	0.18	0.00	0.9879	0.9056	0.7691
13	0.278	0.40	0.00	0.53	0.7881	0.6087	0.6354
14	0.357	0.05	0.43	0.19	0.5848	0.8592	0.7228
15	0.290	0.43	0.04	0.46	0.7548	0.6322	0.7196
Average value	0.375	0.37	0.25	0.45	0.7790	0.6450	0.6463
Relative weight					0.38	0.31	0.31

Abbreviations: GRC refers to grey relational coefficient.

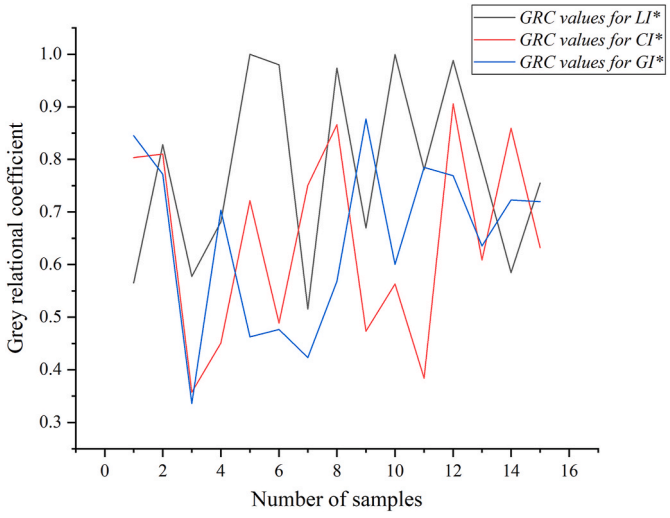

Fig. 9. Grey relational coefficient distribution of different samples. GRC refers to the grey relational coefficient.

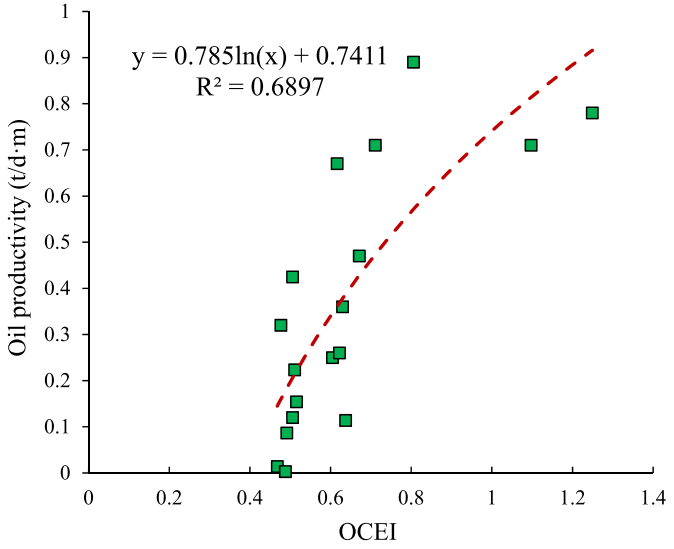

Fig. 10. Crossplot of shale oil productivity and OCEI in the Jimusaer Sag. Shale oil productivity is the result of the daily output divided by the thickness of reservoirs.

zones. Compared with the upper oil tested interval, the single well in the lower oil tested interval has higher daily oil production. This could be due to the influence of the dissolved gas content of the region, which ranges from 321 to 4405 ppm with an average value of 1907 ppm, higher than the value of 818 ppm observed in the upper oil tested interval and indicating high mobility (Table 5). The results obtained using the OCEI method also show that the lower oil tested interval is the most favorable target interval of the well; this indicates the new method is successfully implemented to predict pay zones in the unconventional reservoirs.

6.2. *Well J36*

The second example is well J36. Compared with well J174, well J36 is a commercial well producing 11.82 tons per day in the Lucaogou Formation (Xu et al., 2019). The location of well J36 is shown in Fig. 3.

The vertical distribution of oil saturation, porosity, *LI**, *GI** and OCEI is predicted in the Lucaogou Formation of well J36 using conventional logging curves, as shown in Fig. 12. Although limited core analysis is available, the interval from 4209 to 4255 m (11115-11171 ft) is perforated for oil production (the pink box area in Fig. 12). The oil content evaluation results show that this interval is characterized by the high content of liquid and gaseous hydrocarbons, which is a favorable pay zone (Table 5). The result of oil testing in this zone shows that the production is 11.82 tons per day, which provides sufficient evidence for testing the OCEI method to evaluate the oil content prediction of shale oil systems. The content of liquid hydrocarbons and gaseous hydrocarbons is much larger than that of well J174 (Table 5 and Fig. 12), resulting in relatively high production of well J36. The interval from 4132 to 4140 m (13552.96–13579.20 ft) can also be another potentially favorable interval based on Jarvie's method (Jarvie, 2012) (Fig. 12). Although this interval is characterized by high values of S_1 and chloroform extractable content, the zone shows low liquid hydrocarbon content (*LI** is only 0.87% on average), relatively low gaseous hydrocarbon content (The total gaseous hydrocarbon content is only 5992.68 ppm on average) and thin thickness, indicating that this zone is not a good target area. The depth interval range from 4145.92 to 4199.83 m (13598.62–13775.44 ft) with the OCEI greater than 0.39 in the Luchaogou Formation of well J36 could serve as another potential pay zone, as shown in Fig. 12.

To summarize, as an innovative method proposed in this article, the OCEI method has the following strengths compared with previously

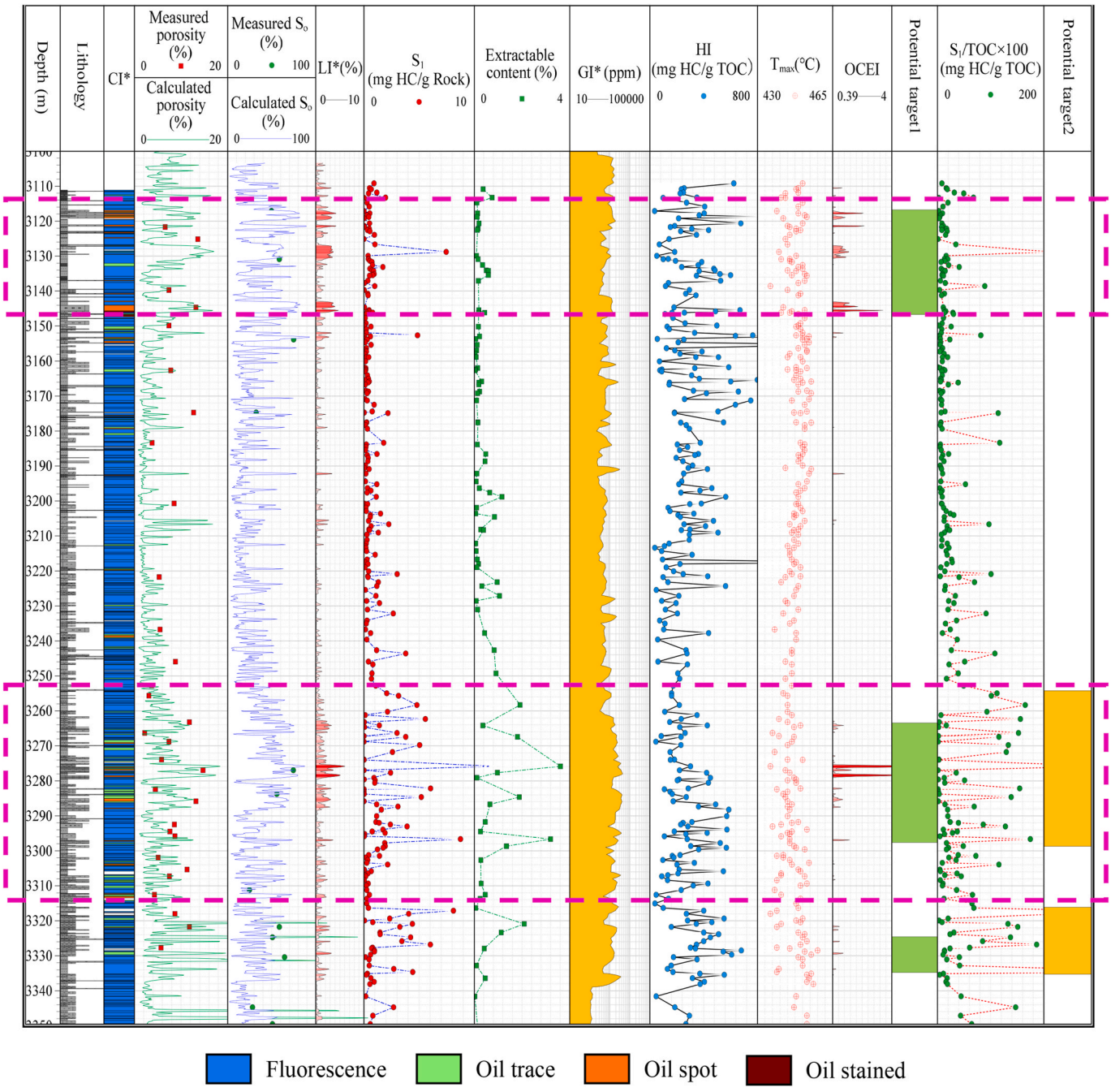

Fig. 11. Prediction of the vertical distribution of potential favorable intervals of the Lucaogou Formation in well J174 of the Jimusaer Sag. S_1 = the volatile hydrocarbon content; OCEI = the oil content evaluation index; *LI** = the oil content evaluation index-related liquid components; *GI** = the oil content evaluation index-related gas components; *CI** = the oil content evaluation index-related core description; Track potential target1 = the favorable reservoir intervals determined by the OCEI method; Track potential target2 = the favorable reservoir intervals determined by the hydrocarbon expulsion threshold proposed by Jarvie (2012). The areas surrounded by the pink box are the formation testing zones. (For interpretation of the references to color in this figure legend, the reader is referred to the Web version of this article.)

available methods. (1) It combines the liquid and gaseous hydrocarbon content in geological conditions. Among them, high liquid hydrocarbon content often means high porosity, high oil saturation and high ρ_{HC}/ρ_b eliminating the situation where only high porosity or high oil content is considered. Mud gas logging data are used to characterize the relative variation in light hydrocarbon (C1–C5) content under geologic conditions. Finally, the relative importance of each parameter is determined by using actual production data based on grey relational analysis. In this way, the method is more reliable and effective. (2) The determination of the threshold value of the OCEI is consistent with the actual production of shale oil under the existing technical conditions. When the OCEI value of a certain interval is higher than the threshold, then the interval is a pay zone. This method can accurately predict the best perforation positions for different wells. (3) This OCEI method provides a high-resolution (0.125m per sample) oil content distribution evaluation model, even if there is no core available.

7. Conclusions

At present, although many methods of characterizing oil content are

Table 4
Rock-Eval pyrolysis, oil saturation, total porosity and chloroform extraction data for core samples from the Lucaogou Formation in well J174.

Depth (m)	Strata	TOC (%)	T_{max} (°C)	S_1 (mg/g)	S_2 (mg/g)	HI (mg/g)	Extraction (%)	Por (%)	So (%)
3109.22	P2l21	10.85	451	0.91	67.74	624			
3110.53	P2l22	3.05	449	0.51	7.79	255			
3110.88	P2l22	3.55	448	0.66	8.35	235	0.37		
3111.87	P2l22	3.68	449	1.17	9.20	250			
3112.09	P2l22	0.85	443	0.42	1.92	226			
3113.30	P2l22	2.89	441	1.96	10.11	350	0.75		
3113.34	P2l22	0.72	443	0.02	0.71	99			
3114.73	P2l22	1.42	451	0.28	3.87	273	0.11		
3115.87	P2l22	4.66	449	0.49	19.00	408			
3117.10	P2l22	0.39	439	0.01	0.14	36			49.7
3117.75	P2l22	5.57	449	0.53	22.48	404	0.14		
3118.33	P2l22	5.32	452	0.29	19.55	367			
3118.78	P2l22	9.77	453	0.44	78.96	808	0.12		
3119.23	P2l22	0.65	442	0.02	1.39	214			
3120.64	P2l22	6.06	451	0.51	40.98	676	0.20		
3121.38	P2l22	0.27	444	0.03	0.50	185			
3121.68	P2l22	0.64	445	0.05	0.98	153		6.60	
3122.14	P2l22	2.84	448	0.49	8.85	312	0.16		
3122.58	P2l22	3.96	450	0.33	17.32	437	0.13		
3122.87	P2l22	2.96	448	0.54	6.81	230			
3123.91	P2l22	6.14	445	0.95	21.30	347			
3125.08	P2l22	0.92	443	0.01	1.32	143		13.60	
3126.61	P2l22	2.89	444	1.00	2.06	71			
3128.78	P2l22	3.51	440	7.46	6.48	185			
3129.90	P2l22	2.30	448	0.38	1.20	52	0.09		
3130.76	P2l22	3.03	445	0.40	4.16	137			
3130.85	P2l22	2.11	441	0.41	2.12	100	0.16		58.6
3131.34	P2l22	4.00	445	0.55	7.64	191			
3131.65	P2l22	10.58	446	0.73	40.86	386			
3132.58	P2l22	3.65	451	0.77	13.13	360	0.35		
3133.16	P2l22	4.21	449	1.72	9.96	237			
3133.64	P2l22	7.58	451	0.54	36.06	476			
3134.05	P2l22	6.77	444	0.74	32.75	484	0.50		
3134.21	P2l22	6.05	448	0.88	22.19	367	0.59		
3135.11	P2l22	10.12	452	0.93	52.68	521			
3135.41	P2l22	9.34	446	0.80	56.02	600	0.59		
3135.56	P2l22	4.48	453	0.51	15.54	347			
3137.01	P2l22	6.25	452	0.36	32.90	526	0.17		
3137.70	P2l22	0.34	449	0.05	0.47	138			
3138.59	P2l22	1.10	436	0.98	1.29	117			
3139.70	P2l22	0.72	444	0.03	2.12	294		7.40	
3140.74	P2l22	2.58	450	0.34	6.89	267			
3141.24	P2l22	4.91	449	0.38	16.84	343			
3144.66	P2l22	0.55	442	0.06	0.99	180		13.20	
3145.44	P2l22	3.73	452	0.47	24.99	670	0.19		
3145.79	P2l22	2.97	446	0.47	14.50	488			
3146.16	P2l22	2.72	441	0.79	6.98	257	0.44		
3146.19	P2l22	1.88	445	0.25	3.11	165	0.18		
3146.54	P2l22	0.76	449	0.23	0.86	113			
3147.68	P2l22	1.07	452	0.12	1.84	172			
3149.22	P2l22	2.26	450	0.20	5.92	262			
3149.82	P2l22	0.93	449	0.02	4.63	498		7.40	
3150.20	P2l22	2.48	448	0.64	3.20	129	0.17		
3150.87	P2l22	2.82	450	0.23	4.08	145			
3151.89	P2l22	3.21	451	0.23	10.69	333			
3152.63	P2l22	5.96	448	4.86	249.57	765			
3152.82	P2l22	3.17	451	0.02	20.20	637			
3152.98	P2l22	13.86	454	0.59	152.17	1098	0.22		
3153.65	P2l22	2.14	453	0.12	1.20	56	0.06		
3153.80	P2l22	1.28	451	0.30	3.24	253			74.8
3154.64	P2l22	1.97	454	0.12	4.15	211			
3155.32	P2l22	12.42	452	0.65	176.00	1417	0.12		
3156.29	P2l22	2.33	449	0.23	2.88	124			
3156.94	P2l22	2.32	453	0.15	4.32	186	0.10		
3157.25	P2l22	5.24	453	0.23	20.35	388			
3157.93	P2l22	0.55	445	0.07	1.24	225	0.04		
3158.88	P2l22	2.54	444	0.24	12.95	510	0.08		
3158.89	P2l22	2.23	450	0.43	7.62	342			
3160.05	P2l22	1.64	451	0.15	1.18	72			
3161.75	P2l22	1.85	448	0.02	10.85	586			
3162.02	P2l22	3.22	453	0.17	10.76	334	0.14		
3162.39	P2l22	1.44	444	0.16	1.30	90	0.05		
3162.62	P2l22	1.08	448	0.15	0.81	75	0.03	7.80	
3162.96	P2l22	1.10	450	0.09	0.98	89			

(*continued on next page*)

Table 4 (*continued*)

Depth (m)	Strata	TOC (%)	T_{max} (°C)	S_1 (mg/g)	S_2 (mg/g)	HI (mg/g)	Extraction (%)	Por (%)	So (%)
3164.06	P2l22	3.53	448	0.32	10.99	311			
3165.04	P2l22	6.95	450	0.41	25.58	368			
3165.32	P2l22	0.67	447	0.05	5.35	799			
3165.87	P2l22	8.19	455	0.48	49.23	601	0.31		
3166.19	P2l22	0.95	451	0.37	1.39	146	0.19		
3166.74	P2l22	0.77	448	0.54	1.98	257	0.19		
3166.74	P2l22	0.59	449	0.12	0.85	144			
3168.48	P2l22	4.45	453	0.19	14.40	324			
3168.69	P2l22	4.02	449	0.40	26.44	658	0.23		
3169.19	P2l22	4.03	455	0.28	16.96	421	0.14		
3170.84	P2l22	1.52	454	0.09	3.92	258			
3171.29	P2l22	3.65	446	0.30	27.38	750	0.10		
3172.45	P2l22	11.83	452	0.93	75.28	636			
3174.40	P2l22	5.28	453	0.75	26.76	507			
3174.75	P2l22	0.43	447	0.03	0.79	184		12.70	32.3
3174.92	P2l22	1.91	450	2.18	3.50	183			
3177.55	P2l22	3.90	448	0.26	21.37	548	0.15		
3177.57	P2l22	3.39	455	0.21	7.80	230	0.15		
3178.34	P2l22	2.52	452	0.14	6.82	271			
3179.37	P2l22	3.69	452	0.32	10.86	294			
3183.36	P2l22	1.53	450	1.79	5.75	376		3.80	
3183.80	P2l22	3.85	452	0.22	7.85	204	0.13		
3184.55	P2l22	3.58	451	0.18	10.05	281			
3185.44	P2l22	2.10	452	0.15	4.66	222			
3186.56	P2l22	5.60	451	1.18	20.14	360	0.48		
3186.91	P2l22	3.00	449	0.30	10.04	335			
3187.70	P2l22	5.13	450	0.39	10.03	196			
3188.62	P2l22	2.92	449	0.36	7.18	246	0.45		
3189.83	P2l22	2.67	451	0.14	8.50	318			
3190.57	P2l22	0.57	443	0.04	1.63	286			
3190.88	P2l22	6.09	455	0.47	26.07	428			
3192.14	P2l22	1.87	454	0.18	4.72	252	0.11		
3194.39	P2l22	2.21	453	0.14	5.23	237	0.08		
3195.18	P2l22	2.22	449	1.17	4.79	216			
3196.30	P2l22	6.99	452	0.32	32.23	461	0.21		
3197.00	P2l22	7.05	450	0.63	26.32	373			
3197.57	P2l22	4.35	448	0.29	10.06	231	0.65		
3198.81	P2l22	12.31	449	1.12	69.48	564	1.16		
3200.73	P2l22	0.53	449	0.04	2.03	383		8.50	
3200.90	P2l22	3.77	448	0.33	11.18	297			
3201.96	P2l22	1.56	450	0.18	2.12	136	0.10		
3202.91	P2l22	1.28	451	0.21	1.92	150			
3203.56	P2l22	6.23	447	1.51	20.36	327	0.06		
3204.01	P2l11	1.92	448	0.59	4.03	210			
3204.57	P2l11	4.46	447	0.58	10.11	227	0.85		
3205.67	P2l11	3.31	452	0.42	15.67	473			
3206.62	P2l11	2.32	445	2.25	5.91	255			
3207.18	P2l11	3.54	450	0.65	14.65	414			
3208.16	P2l11	2.47	449	0.45	7.37	298	0.27		
3208.33	P2l11	2.22	447	0.51	5.19	234	0.39		
3209.07	P2l11	9.97	446	1.31	50.57	507			
3209.61	P2l11	3.65	449	0.27	10.72	294			
3211.09	P2l11	3.26	447	0.28	9.54	293			
3212.16	P2l11	1.13	449	0.21	1.62	143	0.06		
3212.87	P2l11	1.40	444	0.11	1.53	109			
3213.40	P2l11	0.83	447	0.18	0.31	37			
3214.30	P2l11	1.46	445	0.24	1.29	88	0.08		
3215.32	P2l11	5.61	445	1.02	17.64	314			
3216.70	P2l11	1.08	446	0.29	1.03	95	0.13		
3217.51	P2l11	0.36	448	0.10	5.17	1436			
3217.98	P2l11	2.05	447	0.36	4.60	224	0.18		
3218.97	P2l11	1.57	450	0.10	1.92	122	0.11		
3220.08	P2l11	3.09	445	0.43	5.47	177			
3220.85	P2l11	2.99	446	3.01	7.41	248			
3221.50	P2l11	6.56	450	0.34	28.23	430			
3221.79	P2l11	0.91	443	0.37	0.90	99		5.30	
3223.23	P2l11	1.88	441	1.31	2.53	135	0.96		
3224.28	P2l11	7.93	449	1.17	44.66	563	0.32		
3225.47	P2l11	0.95	448	0.13	0.46	48			
3227.14	P2l11	3.23	447	1.09	6.98	216	1.06		
3228.53	P2l11	1.14	443	0.24	1.02	89	0.08		
3229.18	P2l11	4.54	444	1.41	8.87	195			
3231.04	P2l11	1.60	449	0.32	1.85	116	0.14		
3232.14	P2l11	2.91	442	2.66	5.96	205			
3234.19	P2l11	0.78	447	0.28	0.57	73			
3235.05	P2l11	1.38	445	0.21	1.54	112			

(*continued on next page*)

Table 4 (*continued*)

Depth (m)	Strata	TOC (%)	T_{max} (°C)	S_1 (mg/g)	S_2 (mg/g)	HI (mg/g)	Extraction (%)	Por (%)	So (%)
3236.69	P2l11	0.58	438	0.14	0.60	103		5.50	
3237.77	P2l11	6.44	448	0.61	28.16	437	0.43		
3239.57	P2l11	0.70	448	0.26	0.41	59			
3242.61	P2l11	4.38	446	1.15	11.78	269	0.83		
3243.60	P2l11	3.51	446	3.79	9.68	276			
3245.89	P2l11	0.80	443	0.41	0.49	61		8.80	
3246.73	P2l11	3.71	446	0.81	10.39	280			
3249.31	P2l11	1.86	446	0.73	3.86	208	0.91		
3250.82	P2l11	3.96	443	0.68	8.80	222			
3252.81	P2l11	2.17	446	1.07	3.77	174		3.70	
3254.94	P2l11	1.85	442	2.07	3.00	162			
3255.72	P2l11	3.10	444	3.14	5.03	162		3.10	
3258.28	P2l11	2.91	444	4.80	6.37	219	1.92		
3260.25	P2l12	2.30	444	2.14	2.56	111			
3261.23	P2l12	1.81	446	0.12	6.35	351			
3262.30	P2l12	3.57	440	5.57	8.32	233			
3263.19	P2l12	1.21	444	0.04	1.79	148		11.80	
3264.16	P2l12	8.35	450	1.40	35.64	427	0.36		
3264.65	P2l12	2.17	447	0.05	4.83	223			
3266.32	P2l12	1.97	437	3.00	5.17	262		2.20	
3267.19	P2l12	0.55	440	0.01	0.47	85			
3267.47	P2l12	3.28	447	3.79	7.61	232	1.81		
3268.81	P2l12	0.69	446	0.01	0.31	45		7.40	
3269.74	P2l12	3.79	444	5.05	8.74	231			
3271.74	P2l12	2.00	438	2.59	3.01	151			
3273.95	P2l12	0.35	444	0.01	0.64	183		5.80	
3274.00	P2l12	0.45	451	0.01	0.69	153			
3275.87	P2l12	3.71	436	11.70	11.22	302	3.61		
3276.99	P2l12	0.82	443	0.01	1.81	221		14.70	74.5
3277.65	P2l12	6.83	445	2.42	28.82	422	0.97		
3279.11	P2l12	7.09	447	0.91	31.88	450	0.11		
3279.57	P2l12	1.27	448	0.02	2.75	217			
3279.83	P2l12	1.98	444	1.01	4.03	204			
3280.53	P2l12	7.12	448	0.98	30.99	435			
3282.14	P2l12	3.91	450	6.04	11.19	286			
3282.37	P2l12	0.75	439	0.01	0.81	108		4.50	
3283.09	P2l12	0.59	444	0.01	0.89	151			
3283.74	P2l12	0.61	442	0.02	1.02	167			55.7
3284.63	P2l12	3.75	443	5.20	10.16	271	1.89		
3285.81	P2l12	0.61	444	0.01	1.06	174		13.20	
3286.70	P2l12	8.16	446	1.16	39.94	489	0.66		
3287.39	P2l12	4.46	444	3.08	16.16	362			
3288.27	P2l12	8.18	445	1.58	48.05	587			
3290.10	P2l12	5.88	444	1.15	33.63	572			
3291.79	P2l12	4.58	449	1.09	14.34	313	0.46		
3292.01	P2l12	3.50	446	1.38	8.66	247			
3292.49	P2l12	2.79	441	2.40	6.42	230		8.60	
3293.05	P2l12	3.06	437	3.91	8.67	283			
3293.90	P2l12	15.51	453	1.73	88.80	573			
3294.48	P2l12	2.01	446	0.75	3.65	182	0.26	7.60	
3294.86	P2l12	6.79	444	1.92	28.92	426			
3295.24	P2l12	0.53	445	0.07	1.42	268			
3295.85	P2l12	0.83	441	0.04	0.90	108		8.70	
3296.61	P2l12	5.01	445	8.75	13.92	278	3.20		
3297.75	P2l12	10.96	445	1.88	57.32	523			
3298.64	P2l12	3.97	447	1.93	12.05	304	1.35		
3299.10	P2l12	8.42	448	1.74	47.89	569			
3299.63	P2l12	7.28	452	1.23	26.39	363			
3301.19	P2l12	1.10	442	0.43	2.48	225			
3301.42	P2l12	1.95	439	1.41	3.25	167			
3301.93	P2l12	0.65	442	0.14	1.16	178		5.10	
3302.68	P2l12	0.97	445	0.34	0.94	97	0.28		
3303.48	P2l12	2.84	454	0.26	9.40	331			
3303.92	P2l12	1.86	446	2.15	3.75	202			
3305.33	P2l12	0.65	449	0.03	1.42	218		11.30	
3305.88	P2l12	11.65	450	0.66	63.68	547			
3306.47	P2l12	0.98	441	0.36	2.06	210			
3306.97	P2l12	0.65	441	0.09	0.87	134			
3307.28	P2l12	0.38	452	0.17	0.34	89		7.50	
3308.42	P2l12	0.56	439	0.03	0.74	132			
3309.40	P2l12	3.76	453	0.39	16.24	432	0.29		
3309.89	P2l12	2.35	450	0.22	7.58	323			
3311.18	P2l12	0.72	438	0.26	1.68	233			24.7
3312.59	P2l12	0.76	441	0.50	0.36	47	0.46	4.30	
3313.65	P2l12	2.20	450	0.27	3.06	139	0.25		
3315.07	P2l12	0.40	448	0.26	0.15	38			

(*continued on next page*)

Table 4 (*continued*)

Depth (m)	Strata	TOC (%)	T_{max} (°C)	S_1 (mg/g)	S_2 (mg/g)	HI (mg/g)	Extraction (%)	Por (%)	So (%)
3316.35	P2l12	0.60	449	0.41	0.60	100	0.06		
3317.09	P2l12	2.47	439	8.11	9.91	401			
3318.01	P2l12	1.77	436	4.06	4.81	272		8.70	
3319.35	P2l12	11.63	451	2.34	64.20	552			
3319.96	P2l12	1.62	448	0.05	4.55	281			
3320.44	P2l12	9.22	450	0.80	42.52	461			
3320.91	P2l12	3.31	441	4.39	11.45	346	2.09		
3321.77	P2l12	2.16	439	3.26	3.46	160		11.80	58.6
3323.38	P2l12	4.72	449	1.46	18.91	401	1.13		
3323.82	P2l12	6.21	452	1.47	31.76	511			
3324.73	P2l12	3.08	451	4.23	13.86	450			50.8
3325.85	P2l12	4.05	453	3.44	16.20	400			
3326.83	P2l12	3.23	450	6.02	11.21	347			
3327.65	P2l12	1.29	439	0.78	3.90	302		5.70	
3327.94	P2l12	2.91	445	0.69	9.86	339	0.42		
3328.48	P2l12	7.21	458	0.96	49.03	680			
3328.77	P2l12	7.22	452	0.95	39.39	546			
3329.68	P2l12	5.56	455	0.60	33.82	608			
3330.38	P2l12	0.34	449	0.14	0.60	176			64.5
3331.06	P2l12	2.68	451	0.47	9.40	351			
3332.81	P2l12	1.17	451	0.49	1.86	159	0.09		
3333.76	P2l12	1.04	440	2.71	1.36	131			
3334.68	P2l12	1.32	439	4.42	2.27	172			
3335.16	P2l12	2.76	455	0.31	10.28	372			
3335.41	P2l12	5.30	453	0.22	29.30	553			
3336.38	P2l12	3.52	454	0.64	11.16	317	0.46		
3337.43	P2l12	5.82	453	0.93	23.63	406			
3338.10	P2l12	2.93	456	0.55	10.95	374			
3341.56	P2l12	0.36	448	0.16	0.17	47	0.02		
3344.75	P2l12	1.83	447	2.69	3.41	186			28.2
3347.14	P2l12	1.86	453	0.81	5.46	294			
3349.50	P2l12	0.90	453	0.58	2.41	268			50.8
3352.73	P2l12	2.73	459	0.40	10.39	381			
3355.65	P2l12	2.47	455	0.54	6.32	256	0.21		
3359.72	P2j	1.43	451	0.36	1.41	99	0.06		
3362.42	P2j	0.66	448	0.09	0.35	53			
3365.32	P2j	0.44	446	0.25	0.17	39			
3378.42	P2j	0.25	451	0.13	0.02	8	0.01		
3379.18	P2j	0.09	443	0.01	0.02	22			
3380.07	P2j	0.08	448	0.03	0.01	13			
3381.38	P2j	0.09	453	0.04	0.01	11			
3384.99	P2j	0.17	444	0.10	0.01	6	0.01	3.20	
3386.18	P2j	0.16	458	0.04	0.01	6			
3387.40	P2j	0.27	441	0.06	0.02	7			
3388.32	P2j	0.11	460	0.14	0.01	9	0.00		
3392.77	P2j	0.21	441	0.17	0.01	5	0.01		
3422.36	P2j	0.03	447	0.05	0.03	100			
3423.77	P2j	0.61	434	0.32	1.18	193			
3424.42	P2j	0.28	428	0.02	0.58	207		11.40	
3425.53	P2j	0.46	432	0.48	1.46	317			
3425.86	P2j	0.06	437	0.19	0.04	67			
3426.86	P2j	0.47	436	0.65	1.83	389			
3428.55	P2j	0.23	437	0.06	0.48	209			
3429.13	P2j	0.33	434	0.17	0.71	215			
3429.93	P2j	0.25	430	0.02	0.44	176			
3430.97	P2j	0.34	433	0.02	0.64	188			
3431.48	P2j	0.14	427	0.02	0.16	114			
3432.05	P2j	0.22	424	0.18	0.37	168			
3433.28	P2j	0.44	426	0.60	1.59	361			
3433.67	P2j	0.73	436	1.49	2.72	373		8.70	
3435.78	P2j	1.17	431	2.91	4.22	361			
3436.68	P2j	0.39	434	0.33	1.12	287			
3437.38	P2j	0.29	431	0.19	0.51	176			
3438.08	P2j	0.08	442	0.01	0.03	38			
3440.09	P2j	0.05	449	0.02	0.02	40		6.60	

Table 5
Characteristics of the oil testing intervals in well J174 and J36.

Well	Oil testing section (m)	S_o (%)	Por (%)	*LI** (mg HC/g Rock)	*CI**	GI (ppm)	OCEI
J174	3116–3146	5.90–89.10 (44.80)	1.20–17.00 (7.27)	0.04–4.73 (1.48)	1-4 (1.49)	284-1950 (818)	0.23–3.46 (0.51)
J174	3255–3314	3.60–87.62 (41.34)	1.10–18.40 (6.01)	0.03–6.04 (1.10)	1-4 (1.31)	321-4405 (1907)	0.23–8.51 (0.46)
J36	4209–4255	3.20–97.80 (48.83)	0.70–16.30 (6.95)	0.01–4.04 (1.41)	1-3 (1.75)	1185-685650(16398)	0.27–31.69 (1.11)

Abbreviations: S_o = oil saturation; Por = total porosity; A-B (C) = A refers to the minimum value, B refers to the maximum value, C refers to the average value.

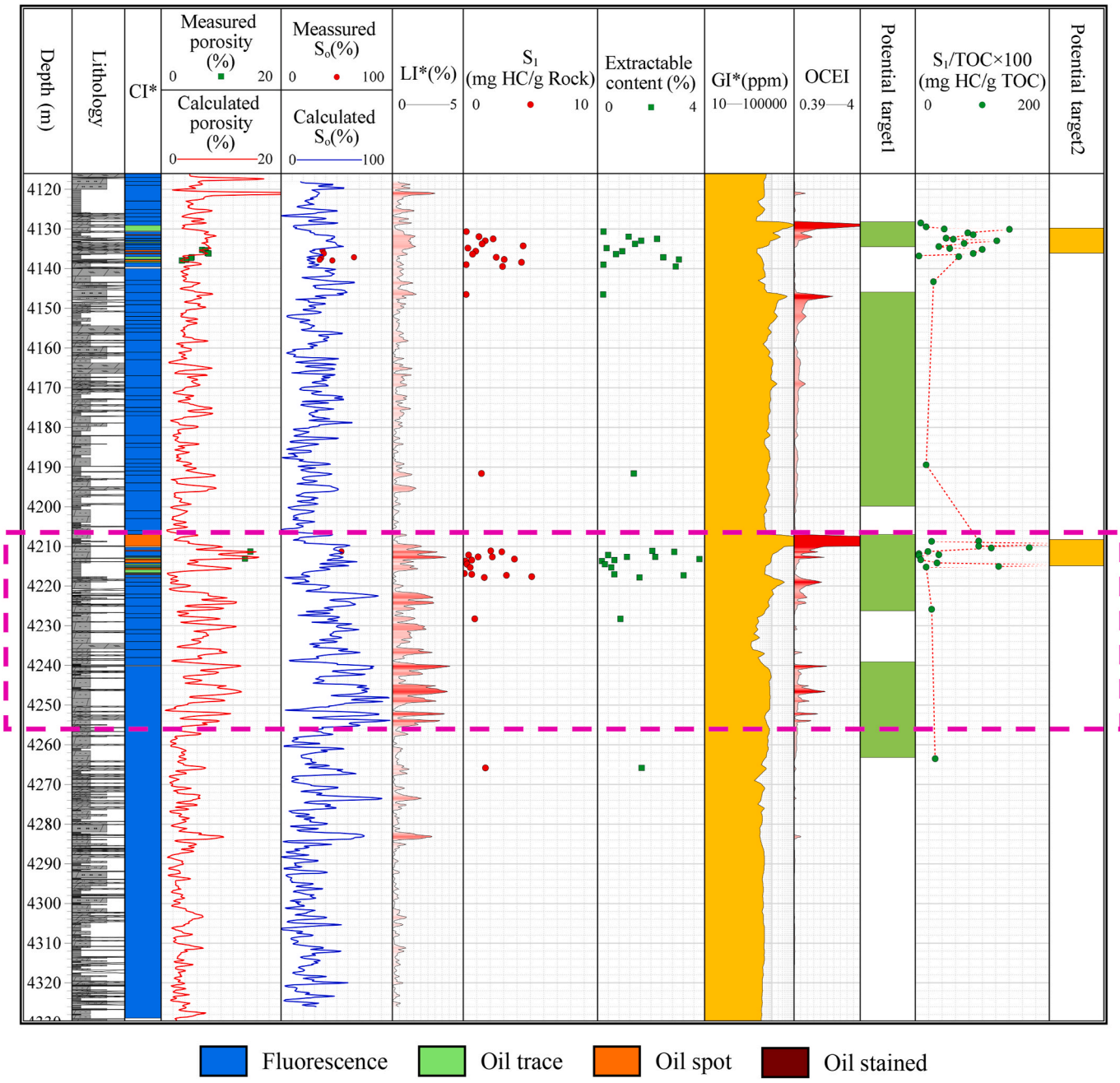

Fig. 12. Prediction of the vertical distribution of potential favorable intervals of the Lucaogou Formation in well J36 of the Jimusaer Sag. S_1 = the volatile hydrocarbon content; OCEI = the oil content evaluation index; *LI** = the oil content evaluation index-related liquid components; *GI** = the oil content evaluation index-related gas components; *CI** = the oil content evaluation index-related core description; Track potential target1 = the favorable reservoir intervals determined by the OCEI method; Track potential target2 = the favorable reservoir intervals determined by the hydrocarbon expulsion threshold proposed by Jarvie (2012).

available, these approaches often address only a certain portion of the characteristics of shale oil composition. In this work, a method (OCEI) for evaluating the oil content of shale oil systems is proposed; this method integrates conventional logging, core description and analytical data. The evaluation index *LI** represents the content of liquid hydrocarbons per unit mass of rock and successfully characterizes the discrete experimental data S_1 and chloroform extraction. Evaluation index *CI** represents the oil-bearing area under the core description. Evaluation index *GI** characterizes the content of gaseous hydrocarbons per unit volume of rock. Among them, the relative weight (importance) of each variable is obtained using the grey relational analysis method. The threshold value of the OCEI applied to determine the pay zones was assigned as 0.39 through its correlation with the production. The results of oil content evaluation in well J174 and J36 based on this new method demonstrated the potential of the method for estimating oil content in shale oil systems.

The oil content evaluation results of OCEI are high-resolution, rapidly obtained and easily interpreted. Controlled by many factors such as sediment composition, diagenesis and migration, the oil content in the shale oil systems is highly heterogeneous. Interesting, not all reservoirs of overlying/underlying source rocks in shale-oil systems show traces of hydrocarbon. The oil content evaluation results obtained with this method will be beneficial in comprehensively analyzing the factors that influence the differential accumulation of shale oil. An additional advantage of this method is that potential reservoirs can be determined in the absence of core data. It should be noted that this

method fully considers the liquid and gaseous hydrocarbon content in the determination of potential reservoirs. However, other factors such as reservoir brittleness and formation pressure are also essential for shale oil production. Therefore, in the evaluation of risks and targets, these geological characteristics and parameters should be comprehensively considered to establish a more complete evaluation model.

Credit authorn statement

Yazhou Liu: Conceptualization, Methodology, Writing – original draft, Writing – review & editing, Investigation. Jianhui Zeng: Conceptualization, Methodology, Supervision, Funding acquisition, Resources. Guangqing Yang: Validation, Investigation, Visualization. Wanting Jia: Investigation, Visualization. Shengnan Liu: Writing – review & editing, Investigation. Xiangye Kong: Writing – review & editing. Shengqian Li: Writing – review & editing, Visualization.

Declaration of competing interest

The authors declare that they have no known competing financial interests or personal relationships that could have appeared to influence the work reported in this paper.

Acknowledgments

The authors sincerely thank the State Key Laboratory of Petroleum Resources and Prospecting and the Xinjiang Oilfield Company of PetroChina for convenience in data and sample collection. This work was financially supported by the National Natural Science Foundation of China (Grant No. 41972147) and the 2020 AAPG Foundation Grants-in-Aid Program (The Institut Français du Pétrole Grant). We thank editor Barry Katz and the other two anonymous reviewers for their detailed comments, which significantly improved the manuscript.

References

Archie, G.E., 1942. The electrical resistivity log as an aid in determining some reservoir characteristics. Transactions of the AIME 146, 54–62.
Asokan, P., Ravi Kumar, R., Jeyapaul, R., Santhi, M., 2007. Development of multi-objective optimization models for electrochemical machining process. Int. J. Adv. Manuf. Technol. 39, 55–63.
Behar, F., Beaumont, V., Penteado, H.L.D.B., 2001. Rock-Eval 6 technology: performances and developments. Oil Gas Sci. Technol. 56, 111–134.
Bordenave, M.L., 1993. Geochemical methods and tools in petroleum exploration. In: Applied Petroleum Geochemistry. Editions Technip, Paris, pp. 207–216.
Cao, Z., Liu, G., Kong, Y., Wang, C., Niu, Z., Zhang, J., Geng, C., Shan, X., Wei, Z., 2016. Lacustrine tight oil accumulation characteristics: permian Lucaogou Formation in jimusaer sag, Junggar Basin. Int. J. Coal Geol. 153, 37–51.
Cao, Z., Liu, G., Xiang, B., Wang, P., Niu, G., Niu, Z., Li, C., Wang, C., 2017. Geochemical characteristics of crude oil from a tight oil reservoir in the Lucaogou Formation, Jimusar sag, Junggar Basin. AAPG (Am. Assoc. Pet. Geol.) Bull. 101, 39–72.
Castagna, J.P., Batzle, M.L., Kan, T.K., Backus, M.M., 1993. Rock physics—the link between rock properties and AVO response. Offset-dependent reflectivity—Theory and practice of AVO analysis: SEG 8, 135–171.
Çaydaş, U., Hasçalık, A., 2008. Use of the grey relational analysis to determine optimum laser cutting parameters with multi-performance characteristics. Opt Laser. Technol. 40, 987–994.
Chen, Z., Wang, T., Liu, Q., Zhang, S., Zhang, L., 2015. Quantitative evaluation of potential organic-matter porosity and hydrocarbon generation and expulsion from mudstone in continental lake basins: a case study of Dongying sag, eastern China. Mar. Petrol. Geol. 66, 906–924.
Dembicki, H., 2016. Practical Petroleum Geochemistry for Exploration and Production. Elsevier.
Deng, J., 1982. Control problems of grey systems. Syst. Contr. Lett. 1, 288–294.
Du, J., Hu, S., Pang, Z., Lin, S., Hou, L., Zhu, R., 2019. The types, potentials and prospects of continental shale oil in China. China Petroleum Exploration 24, 560–568.
Espitalié, J., Laporte, L., Madec, M., Marquis, F., Leplat, P., Paulet, J., Boutefeu, A., 1977. Méthode rapide de caractérisation des roches mètres, de leur potentiel pétrolier et de leur degré d'évolution. Rev. Inst. Fr. Pet 32, 23–42.
Espitalié, J., Makadi, K.S., Trichet, J., 1984. Role of the mineral matrix during kerogen pyrolysis. Org. Geochem. 6, 365–382.
Gao, G., Zhang, W., Xiang, B., Liu, G., Ren, J., 2016. Geochemistry characteristics and hydrocarbon-generating potential of lacustrine source rock in Lucaogou Formation of the jimusaer sag, Junggar Basin. J. Petrol. Sci. Eng. 145, 168–182.
Gao, Y., Ye, Y., He, J., Qian, G., Qin, J., Li, Y., 2020. Development practice of continental shale oil in Jimsar sag in the Junggar Basin. China Petroleum Exploration 25, 133–141.
Gardner, M.H., Borer, J.M., Melick, J.J., Mavilla, N., Dechesne, M., Wagerle, R.N., 2003. Stratigraphic process-response model for submarine channels and related features from studies of Permian Brushy Canyon outcrops, West Texas. Mar. Petrol. Geol. 20, 757–787.
Glaser, K.S., Miller, C.K., Johnson, G.M., Toelle, B., Kleinberg, R.L., Miller, P., Pennington, W.D., 2013. Seeking the sweet spot: reservoir and completion quality in organic shales. Oilfield Rev. 25, 16–29.
Hackley, P.C., Fishman, N., Wu, T., Baugher, G., 2016. Organic petrology and geochemistry of mudrocks from the lacustrine Lucaogou Formation, Santanghu Basin, Northwest China: application to lake basin evolution. Int. J. Coal Geol. 168, 20–34.
Hakami, A., Ellis, L., Al-Ramadan, K., Abdelbagi, S., 2016. Mud gas isotope logging application for sweet spot identification in an unconventional shale gas play: a case study from Jurassic carbonate source rocks in Jafurah Basin, Saudi Arabia. Mar. Petrol. Geol. 76, 133–147.
Hammerschmidt, S.B., Wiersberg, T., Heuer, V.B., Wendt, J., Erzinger, J., Kopf, A., 2014. Real-time drilling mud gas monitoring for qualitative evaluation of hydrocarbon gas composition during deep sea drilling in the Nankai Trough Kumano Basin. Geochem. Trans. 15, 1–15.
Horsfield, B., 1984. Pyrolysis studies and petroleum exploration. Adv. Petrol. Geochem. 1, 247–298.
Hu, S., Zhao, W., Hou, L., Yang, Z., Zhu, R., Wu, S., 2020. Development potential and technical strategy of continental shale oil in China. Petrol. Explor. Dev. 47, 1–10.
Hu, T., Pang, X., Jiang, S., Wang, Q., Zheng, X., Ding, X., Zhao, Y., Zhu, C., Li, H., 2018a. Oil content evaluation of lacustrine organic-rich shale with strong heterogeneity: a case study of the Middle Permian Lucaogou Formation in Jimusaer Sag, Junggar Basin, NW China. Fuel 221, 196–205.
Hu, T., Pang, X., Wang, Q., Jiang, S., Wang, X., Huang, C., Xu, Y., Li, L., Li, H., 2018b. Geochemical and geological characteristics of permian Lucaogou Formation shale of the well Ji174, Jimusar sag, Junggar Basin, China: implications for shale oil exploration. Geol. J. 53, 2371–2385.
Huang, Z., Liu, G., Li, T., Li, Y., Yin, Y., Wang, L., 2017. Characterization and control of mesopore structural heterogeneity for low thermal maturity shale: a case study of Yanchang Formation Shale, Ordos Basin. Energy Fuels 31, 11569–11586.
Jarvie, D.M., 2008. Unconventional Shale Resource Plays: Shale-Gas and Shale-Oil Opportunities. Texas Chtistian Unversity, Wordwide Geochemistry.
Jarvie, D.M., 2012. Shale Resource Systems for Oil and Gas: Part 2—Shale-Oil Resource Systems.
Jiang, C., Chen, Z., Mort, A., Milovic, M., Robinson, R., Stewart, R., Lavoie, D., 2016. Hydrocarbon evaporative loss from shale core samples as revealed by Rock-Eval and thermal desorption-gas chromatography analysis: its geochemical and geological implications. Mar. Petrol. Geol. 70, 294–303.
Jin, Y., Li, S., Yang, D., 2020. Experimental and theoretical quantification of the relationship between electrical resistivity and hydrate saturation in porous media. Fuel 269, 117378.
Jin, Z., Bai, Z., Gao, B., Li, M., 2019. Has China ushered in the shale oil and gas revolution? Oil Gas Geol. 40, 451–458.
Kolahan, F., Golmezerji, R., Moghaddam, M.A., 2011. Multi objective optimization of turning process using grey relational analysis and simulated annealing algorithm. Appl. Mech. Mater. 110–116, 2926–2932.
Kuang, L.C., Sun, Z.C., Ouyang, M., Chang, Q.S., Wang, Z.L., 2013. Complication lithology logging identification of the Lucaogou tight oil reservoir in Jimusar depression. Well Logging Technol. 37, 638–642.
Kuo, Y., Yang, T., Huang, G.-W., 2008. The use of grey relational analysis in solving multiple attribute decision-making problems. Comput. Ind. Eng. 55, 80–93.
Li, J., Wang, M., Lu, S., Chen, G., Tian, W., Jiang, C., Li, Z., 2020. A new method for predicting sweet spots of shale oil using conventional well logs. Mar. Petrol. Geol. 113, 104097.
Li, J., Wang, W., Cao, Q., Shi, Y., Yan, X., Tian, S., 2015. Impact of hydrocarbon expulsion efficiency of continental shale upon shale oil accumulations in eastern China. Mar. Petrol. Geol. 59, 467–479.
Li, W., Lu, S., Xue, H., Zhang, P., Hu, Y., 2015. Oil content in argillaceous dolomite from the Jianghan Basin, China: application of new grading evaluation criteria to study shale oil potential. Fuel 143, 424–429.
Lin, C.-T., Chang, C.-W., Chen, C.-B., 2006. The worst ill-conditioned silicon wafer slicing machine detected by using grey relational analysis. Int. J. Adv. Manuf. Technol. 31, 388–395.
Liu, C., Liu, K., Wang, X., Wu, L., Fan, Y., 2019a. Chemostratigraphy and sedimentary facies analysis of the permian Lucaogou Formation in the jimusaer sag, Junggar Basin, NW China: implications for tight oil exploration. J. Asian Earth Sci. 178, 96–111.
Liu, C., Liu, K., Wang, X., Zhu, R., Wu, L., Xu, X., 2019b. Chemo-sedimentary facies analysis of fine-grained sediment formations: an example from the Lucaogou Fm in the Jimusaer sag, Junggar Basin, NW China. Mar. Petrol. Geol. 110, 388–402.
Lu, S., Xue, H., Wang, M., Xiao, D., Huang, W., Li, J., Xie, L., Tian, S., Wang, S., Li, J., 2016. Several key issues and research trends in evaluation of shale oil. Acta Pet. Sin. 37 (10), 1309–1322.
Luo, X., Wang, Z., Zhang, L., Yang, W., Liu, L., 2007. Overpressure generation and evolution in a compressional tectonic setting, the southern margin of Junggar Basin, northwestern China. AAPG Bull. 91, 1123–1139.
National Standard of practices for core analysis, 2017. 2017 National Standard of Practices for Core Analysis. GB/T 34906–2017, P. R. China.

Noble, R.A., 1991. Geochemical techniques in relation to organic matter: chapter 8: geochemical methods and exploration. Am. Assoc. Petrol. Geol. 97–102.
Peters, K.E., 1986. Guidelines for evaluating petroleum source rock using programmed pyrolysis. AAPG Bull. 70, 318–329.
Qin, Z., Pan, H., Ma, H., Konaté, A.A., Hou, M., Luo, S., 2016. Fast prediction method of Archie's cementation exponent. J. Nat. Gas Sci. Eng. 34, 291–297.
Qiu, Z., Lu, B., Shi, Z., Dong, D., Wang, H., Zhou, J., Tao, H., Zheng, M., Wu, X., Guo, H.-k., 2016a. Residual accumulation and resource assessment of shale oil from the permian Lucaogou Formation in Jimusar sag. Natural Gas Geoscience 27, 1817–1827.
Qiu, Z., Tao, H., Zou, C., Wang, H., Ji, H., Zhou, S., 2016b. Lithofacies and organic geochemistry of the middle permian Lucaogou Formation in the Jimusar sag of the Junggar Basin, NW China. J. Petrol. Sci. Eng. 140.
Raymer, L.L., Hunt, E.R., Gardner, J.S., 1980. An improved sonic transit time-to-porosity transform. In: SPWLA 21st Annual Logging Symposium. SPWLA-1980-P, pp. 1–13.
Shanmugam, G., Bloch, R.B., Mitchell, S.M., Beamish, G.W.J., Hodgkinson, R.J., Damuth, J.E., Straume, T., Syvertsen, S.E., Shields, K.E., 1995. Basin-floor fans in the North Sea: sequence stratigraphic models vs. sedimentary facies. AAPG Bull. 79, 477–512.
Sun, H., Cai, X., Zhou, D., Gao, B., Zhao, P., 2019. Practice and prospect of Sinopec shale oil exploration. China Petroleum Exploration 24, 569–575.
Ter Heege, J., Zijp, M., Nelskamp, S., Douma, L., Verreussel, R., Ten Veen, J., de Bruin, G., Peters, R., 2015. Sweet spot identification in underexplored shales using multidisciplinary reservoir characterization and key performance indicators: example of the Posidonia Shale Formation in The Netherlands. J. Nat. Gas Sci. Eng. 27, 558–577.
Tesson, M., Posamentier, H.W., Gensous, B., 2000. Stratigraphic organization of late pleistocene deposits of the western part of the Golfe du Lion shelf (Languedoc shelf), Western Mediterranean Sea, using high-resolution seismic and core data. AAPG Bull. 84, 119–150.
Tosun, N., 2005. Determination of optimum parameters for multi-performance characteristics in drilling by using grey relational analysis. Int. J. Adv. Manuf. Technol. 28, 450–455.
Wang, M., 2014. Key parameter and calculation in shale oil reservoir evaluation. Acta Sedimentol. Sin. 32, 174–181.
Wang, M., Guo, Z., Jiao, C., Lu, S., Li, J., Xue, H., Li, J., Li, J., Chen, G., 2019. Exploration progress and geochemical features of lacustrine shale oils in China. J. Petrol. Sci. Eng. 178, 975–986.
Wang, M., Tian, S., Chen, G., Xue, H., Huang, A., Wang, W., 2014. Correction method of light hydrocarbons losing and heavy hydrocarbon handling for residual hydrocarbon (S_1) from shale. Acta Geologica Sinica-English Edition 88, 1792–1797.
Wang, X., Yang, Z., Guo, X., Wang, X., Feng, Y., Huang, L., 2019. Practices and prospects of shale oil exploration in Jimsar sag of Junggar basin. Xinjing Pet. Geol. 40, 402–413.
Wang, X.W., Wang, X.W., Ma, Y.S., 2007. The tectonic evolution of Bogda Mountain, Xinjiang, Northwest China and its relationship to oil and gas accumulation. Geoscience 21, 116–124.
Wu, B., Li, J., Wu, Y., Han, L., Zhao, T., Zou, Y., 2019. Development practices of geology-engineering integration on upper sweet spots of Lucaogou Formation shale oil in Jimsar sag, Junggar Basin. China Petroleum Exploration 24, 679–690.
Wu, H., Hu, W., Cao, J., Wang, X., Wang, X., Liao, Z., 2016. A unique lacustrine mixed dolomitic-clastic sequence for tight oil reservoir within the middle Permian Lucaogou Formation of the Junggar Basin, NW China: reservoir characteristics and origin. Mar. Petrol. Geol. 76, 115–132.
Wyllie, M.R.J., Gregory, A.R., Gardner, L.W., 1956. Elastic wave velocities in heterogeneous and porous media. Geophysics 21, 41–70.
Xiao, W., Han, C., Yuan, C., Sun, M., Lin, S., Chen, H., Li, Z., Li, J., Sun, S., 2008. Middle Cambrian to Permian subduction-related accretionary orogenesis of Northern Xinjiang, NW China: implications for the tectonic evolution of central Asia. J. Asian Earth Sci. 32, 102–117.
Xu, L., Chang, Q., Yang, K., 2019. Characteristics and oil-bearing capability of shale oil reservoir in the Permian Lucaogou Formation, Jimusaer sag. Oil Gas Geol. 40, 536–540.
Xue, H.T., Tian, S.S., Wang, W.M., Zhang, W.H., Du, T.T., Mu, G.D., 2016. Correction of oil content-one key parameter in shale oil resource assessment. Oil Gas Geol. 37, 15–22.
Yang, T., Chen, M.-C., Hung, C.-C., 2007. Multiple attribute decision-making methods for the dynamic operator allocation problem. Math. Comput. Simulat. 73, 285–299.
Yang, T., Hung, C.-C., 2007. Multiple-attribute decision making methods for plant layout design problem. Robot. Comput. Integrated Manuf. 23, 126–137.
Zeng, G., Jiang, R., Huang, G., Xu, M., Li, J., 2007. Optimization of wastewater treatment alternative selection by hierarchy grey relational analysis. J. Environ. Manag. 82, 250–259.
Zhang, J., Liu, G., Cao, Z., Tao, S., Felix, M., Kong, Y., Zhang, Y., 2019. Characteristics and formation mechanism of multi-source mixed sedimentary rocks in a saline lake, a case study of the Permian Lucaogou Formation in the Jimusaer Sag, northwest China. Mar. Petrol. Geol. 102, 704–724.
Zhao, P., Wang, Z., Sun, Z., Cai, J., Wang, L., 2017. Investigation on the pore structure and multifractal characteristics of tight oil reservoirs using NMR measurements: permian Lucaogou Formation in Jimusaer Sag, Junggar Basin. Mar. Petrol. Geol. 86, 1067–1081.
Zhao, W., Hu, S., Hou, L., Yang, T., Li, X., Guo, B., Yang, Z., 2020. Types and resource potential of continental shale oil in China and its boundary with tight oil. Petrol. Explor. Dev. 47, 1–10.
Zhao, X., Pu, X., Zhou, L., Jin, F., Shi, Z., Han, W., Jiang, W., Zhang, W., 2020. Typical geological characteristics and exploration practices of lacustrine shale oil: a case study of the Kong-2 member strata of the Cangdong Sag in the Bohai Bay Basin. Mar. Petrol. Geol. 113, 103999.
Zhao, X., Zhou, L., Pu, X., Jin, F., Shi, Z., Xiao, D., 2019. Favorable formation conditions and enrichment characteristics of lacustrine facies shale oil in faulted lake basin: a case study of Member 2 of Kongdian Formation in Cangdong Sag, Bohai Bay Basin. Acta Pet. Sin. 40, 1013–1029.
Zhu, R., Zhang, L., Li, J., Liu, Q., Li, Z., Wang, R., Zhang, L., 2015. Quantitative evaluation of residual liquid hydrocarbons in shale. Acta Pet. Sin. 36, 13–18.
Zhu, R., Zou, C., Wu, S., Yang, Z., Mao, Z., Yang, H., Fan, C., Hui, X., Cui, J., Su, L., 2019. Mechanism for generation and accumulation of continental tight oil in China. Oil Gas Geol. 40, 1168–1184.
Zou, C., Pang, S., Jing, Z., Gao, J., Yang, Z., Wu, S., Zhao, Q., 2020. Shale oil and gas revolution and its impact. Acta Pet. Sin. 41, 1–12.